Evaluation of the optimal working conditions for the warm sheet HydroForming taking into account the yielding condition

Evaluation of the optimal working conditions for the sheet Hydroforming taking into account the yielding condition

Gianfranco Palumbo[1, a], Vito Piglionico[1, b], Antonio Piccininni[1, c], Pasquale Guglielmi[1, d] and Luigi Tricarico[1, e]

[1]DMMM – Politecnico di Bari, viale Japigia 182 – Bari, Italy
[a]gianfranco.palumbo@poliba.it, [b]vito.piglionico@poliba.it, [c]antonio.piccininni@poliba.it, [d]pasquale.guglielmi@poliba.it and [e]luigi.tricarico@poliba.it

Abstract

The present work aims at determining the optimal working condition for the manufacturing of an aluminium (AA6061-T6) component by sheet Hydroforming. The numerical model of the process was developed using the commercial explicit code LS-DYNA; great attention was paid to the material modelling, implementing experimental data in terms of flow curves, anisotropy and forming limit curves; in addition two different yield criteria were adopted: an anisotropic criterion (Barlat '89) and the standard isotropic one (Von Mises).

In order to evaluate the optimal working conditions, a multi-objective optimization procedure was adopted. Process parameters (temperature, blank holder force, oil pressure) were changed in the simulations according to a Central Composite Design and the effects were evaluated monitoring output variables able to take in to account both the die filling and the occurrence of sheet bursting. Results from the optimization were compared and experimentally validated: it is relevant that, irrespective to the tuning of the models with any yield formulation, experimental hydroforming tests confirmed the effectiveness only of the anisotropic Barlat, thus highlighting that the yield criterion strongly affects the results of the optimization procedure.

Keywords: sheet Hydroforming, Al 6xxx series, multi-objective optimization, FE analysis, yield criterion.

1. Introduction

In these last years, mass reduction and limited pollutant emissions are considered the main tasks to be reached by car manufacturers. The adoption of light alloys for lightweighting vehicles is one of the most promising solutions to this problem: Schultz et al. demonstrated that replacing steel by Aluminium (Al) leads to mass reduction ranging from 40 to 60% with a subsequent improvement in fuel efficiency [1] (reducing the mass of the car of 100 kg can save about 9 grams of CO_2 per Km). In order to reduce the weight, car manufacturers largely adopted Al alloy for producing automotive components (bonnets, doors, front structure, wings, crash elements and bumpers) since such an alloy allows a suitable combination of improved surface quality and mechanical properties (30% of weight reduction with no appreciable changing in car performance) [2]. In particular, Al 6xxx series alloy are preferred when high strength and surface quality are needed, whereas Al 5xxx series are adopted when energy absorption and/or higher drawability are necessary [3].

Starting from this scenario, it is quite clear that Al alloy can be considered the most attractive alternative to conventional carbon steel grades, especially for their excellent corrosion resistance. As well known in literature, the main limiting drawback of Al alloys is the poor formability at room temperature, mainly due to the high percentage of alloying elements needed to ensure high mechanical properties [4]: if compared to a traditional deep drawing steel, Al alloys exhibit (in the same working conditions) a formability reduction of almost two thirds. In addition, low formability leads to the necessity of increasing the number of forming step that, in turns, means to limit the massive adoption of such alloys. The abovementioned limitations can be overcome adopting, for example, warm working conditions, able to determine an improvement of the ductility due to the increased strain rate hardening [5] accompanied by both the reduction of the flow stress and the increase of the material toughness [6]; the high strain rate hardening is determinant at elevated temperature (about

300°C) for improving the Forming Limit Curve (FLC) of the material, while at lower temperature (below 200°C) the formability is also strongly affected by the strain-hardening [7]. Another solution for producing lightweight automotive components using Al is to adopt innovative stamping processes, like for example the Sheet HydroForming (SHF): in such a process the punch is replaced by a fluid (oil) under pressure [8-11] and higher level of geometrical complexity and/or strain levels accompanied by a more uniform strain distribution can be obtained. The combination of both the warm conditions and the SHF surely represent a logical consequence of the advantages coming from the above mentioned solutions. One of the drawbacks of the Warm HydroForming (WHF) process is the presence of a more complex working window, since it is affected by a larger number variables than the process at room temperature: Temperature, Blank Holder Force and oil Pressure.

Finite element (FE) simulations offer the possibility to previously investigate the process and the effect of the above mentioned parameters, thus avoiding the trial and error procedure in the process development step; actually, such a technique is successfully applied to: (i) reduce the product design time, (ii) compare design options, (iii) understand the way the process parameters affects the manufacturing process [12]. Main drawback related to the FE approach is the need of tuning the model, in terms of both material and tribology. As concerns the material modelling, it is necessary an accurate mechanical and technological characterization of the Al alloy and, at the same time, the evaluation of the most appropriate Yield Criterion (YC); in addition, in order to properly define the tribological conditions affecting the interaction with tools, usually modelled adopting simple models (Coulomb), it is necessary to correctly tune the Coefficient of Friction (CoF) according to the working conditions. Various solutions are reported in literature for the CoF evaluation: pin-on-disk test represents a well-assessed solution to evaluate the values to be implemented within numerical models [13]; in other cases, the choice of the friction test depends on the investigated forming process. In the

case of tube hydroforming, for example, tube upsetting friction test is usually adopted, based on the consideration that friction influences tube thickness during the process [14-15]. A well-known alternative approach is the adoption of the inverse analysis, based on the minimization of the difference between numerical and experimental data (an output parameter affected by the friction); for example, Korkolis and Kyriakides compared the experimental evolution of the axial strain of a formed tube with the correspondent numerical trend in order to evaluate the CoF value able to best fit experimental data [16].

As concerns the material modelling, the characterization in terms of flow stress curves (according to temperatures and strain rates) and the FLC usually gives a detailed description of the material plastic behaviour; but the way (i.e. the load conditions under which) the material enters in the plastic field has to be properly chosen. The anisotropy of the material can strongly affect the material plasticity, thus making the classical and more largely adopted isotropic Von Mises formulation not suitable when modelling sheet forming processes. Hill, in 1948 [17], proposed a first simple anisotropic yield model in the form of a quadratic function; since then, several formulations have been developed to account for material anisotropy to obtain a better description of the plastic behaviour and, at the same time, answer to the more demanding need of the application field [18-19]. Alternatively, some author proposed new yield criteria, usually extensions of previous issued formulations, that reveal to be more suitable for the investigated specific case of study [20].

On the other hand, great efforts were spent to enhance the process potentiality through several optimization procedures: generally, the most used approach is based on algorithms (in most of cases a gradient based type) to be stopped when convergence is reached [21-22]; their limitation of leading to local optima can be overcome by the adoption of more sophisticated solutions: genetic algorithms as well as simulated annealing algorithms revealed to be more effective [23-25]. One of the most promising procedures involves the

adoption of the Response Surface Methodology (RSM) as a powerful mean to reduce the number of numerical simulations: many examples can be found in literature, like for example the optimization of the stamping process of an automotive component or the control of the springback effects [26-28].

The present work aims to determine the optimal working conditions for the manufacturing of an Al component (AA6061 T6) taking into account the YC; in particular, in this work it is investigated how the YC affects the optimization results. A preliminary experimental campaign was carried out to characterize the investigated alloy in terms of mechanical and technological properties (flow stress curves and FLCs), taking into account the temperature, the strain rate and the orientation with respect to the rolling direction. Results coming from this first phase were implemented in a FE model created using the commercial code LS-Dyna. The plastic behaviour of the investigated alloy was modelled using both an isotropic yield function (Von Mises) and an anisotropic one (Barlat '89). The most influencing process parameters (forming pressure, blankholder force and working temperature) were varied according to a Central Composite Design plan; in addition, results from numerical simulations were collected in terms of response variables in order to create Response Surfaces (RS) to be used for the optimization procedure. In particular, the optimization procedure was performed using at first the von Mises YC, then the anisotropic Barlat '89 YC. Results were compared and experimentally validated in order to understand how the optimal working window is affected by the yielding condition adopted for modelling the material plasticity.

2. Material and Methods

2.1 Mechanical characterization of investigated alloy

A single batch of AA6061, 0.5 mm thick, was purchased in the T6 condition. The chemical composition is presented in Table 1.

Table 1. Chemical composition

Si %	Fe %	Cu %	Mn %	Mg %	Cr %	Zn %	Ti %
0.67	0.42	0.23	0.10	0.92	0.18	0.04	0.07

As concerns the mechanical characterization, dog bone specimens (gauge length: 100 mm; width: 15 mm) were adopted. Three temperature levels (20°C, 110°C and 220°C) were investigated as well as three different orientations with respect to the rolling direction (0°, 45° and 90°). Tensile tests were performed on a 20 tons electromechanical INSTRON tensile test machine, equipped with the specifically designed furnace shown in Figure 1a, able to heat the specimen thanks to 9 radiant heaters positioned around the specimen.

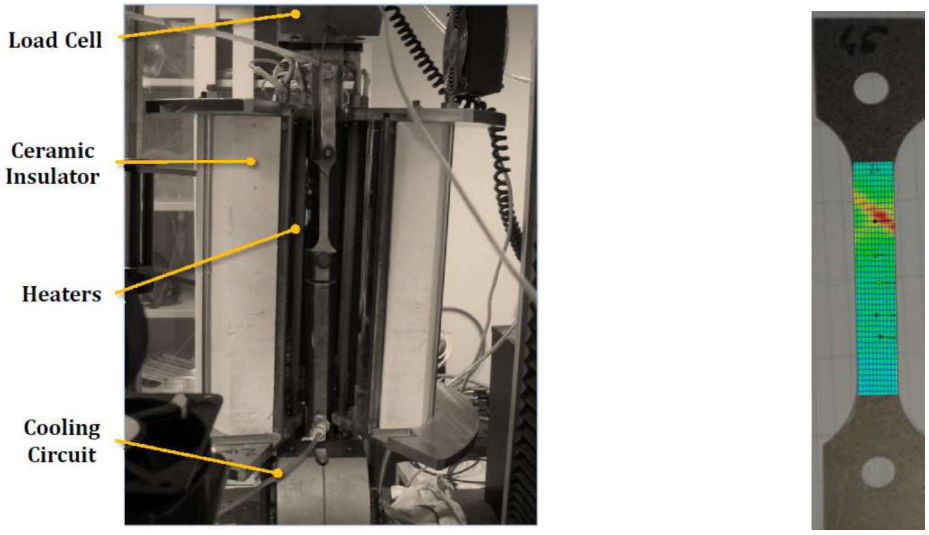

Figure 1: Tensile test equipment: a) heating device; b) example of a strain field acquired by the DIC system

The furnace allowed to monitor the whole test with a non-contact optical 3D measuring system, able to obtain the full-field strain values by means of the Digital Image Correlation (DIC) technique (an example is reported in Figure 1b): specimens were painted in order to create a stochastic pattern on the surface to be used by the DIC system for correlating images and calculate the strain field.

2.2Warm HydroForming facility & Case study

WHF tests were carried out using the facility shown in Figure 2a: it is a 2500 kN electro-hydraulic press machine (4 electric motors supported by additional 2 hydraulic cylinders for increasing the closing force) specifically designed and produced as a prototype.

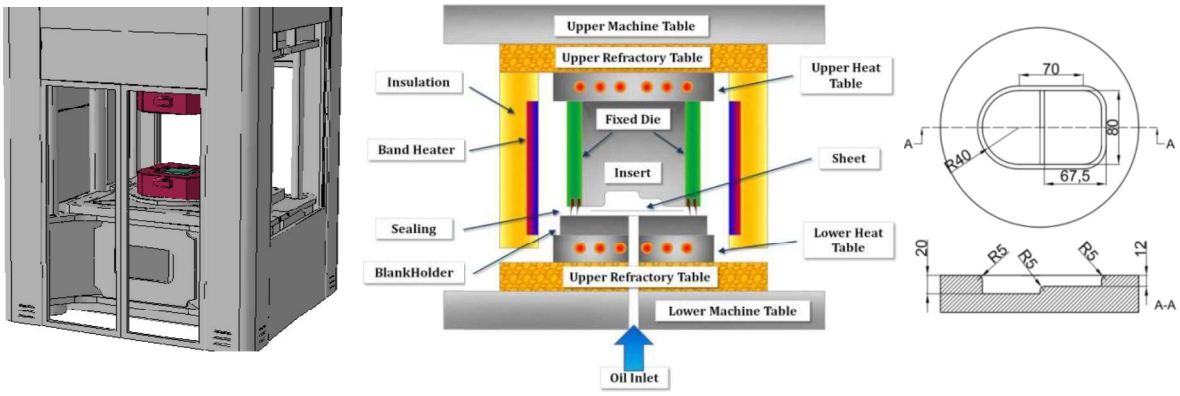

a) b) c)

Figure 2. WHF equipment: a) 3D overview of the Press machine; b) schematic view of the heated tools; c) die insert

The press machine is suitable for both Warm Hydroforming and SuperPlastic Forming tests, being equipped with heated tools for warm (up to 350°C) and hot conditions (up to 1000°C): the press functional scheme is reported in Figure 2b. In the present work the warm working tools were used for the WHF tests. In particular, the lower and the upper tool contain a metallic Blank Holder and a metallic insert (the die) respectively, whose geometry is reported in Figure 2c: it is a stepped die characterised by two depths cavities, respectively equal to 12mm and 20mm. Each tool (both the lower and the upper one) contains a Nichel Alloy 600 element embedding 6 electric cartridges (9kW in the bottom tool and 15kW in the upper tool), managed by the programmable logic control (PLC) of the press machine using temperature data from thermocouples placed near the electric cartridges and also in proximity of both the die surface (upper tool) and the Blank Holder (lower tool). The heating phase is considered completed by the PLC when the temperature difference between the die

cavity and the blank holder is smaller than the specified (5°C in the experiments of this work), thus assuring a uniform temperature distribution. In the present work, investigated temperatures and time exposure were respectively limited to 220°C and 60 s, so that the working condition did not alter the supply condition of the material.

The blank to be formed was introduced into the tools (between the upper die and the Blank Holder) once the system reached the target temperature; no lubricant was used in the experiments. The forming fluid (oil) was introduced through the lower die at the same temperature of the tools; oil pressure was controlled through a proportional electronic valve (maximum pressure: 350 bar) also managed by the PLC in order to reproduce any pressure profile defined by the user.

The DIC system was used to obtain information (strain distribution and thickness reduction) for calibration and validation purposes: the blanks were painted, acquired by the DIC system before being introduced in the die and finally acquired again after deformed in order to compare the stochastic pattern on their surfaces.

2.3 Numerical modelling

The numerical model is shown in Figure 3: it was created adopting the commercial FE Explicit code LS-DYNA, assuming the Blank Holder and the die as rigid parts while the blank as deformable (Belytschko-Tsay shell elements, with five through-thickness integration points [29] were used). As shown in Figure 3, the blank (thickness: 0.5 mm) was divided into two regions: the internal one (A_{OIL}), subjected to the oil pressure, and the external one (A_{BHF}), on which the Blank Holder Force was applied.

As concerns the material plastic behaviour, two different yield criteria were taken into account: the isotropic one (Von Mises formulation) and an anisotropic one (Barlat '89 criterion). The Von Mises YC is considered a general purpose criterion, easy to be

implemented [30]; flow stress curve along the rolling direction was implemented according to Hollomon's model (Equation 1).

$$\sigma = K\varepsilon^n \quad (1)$$

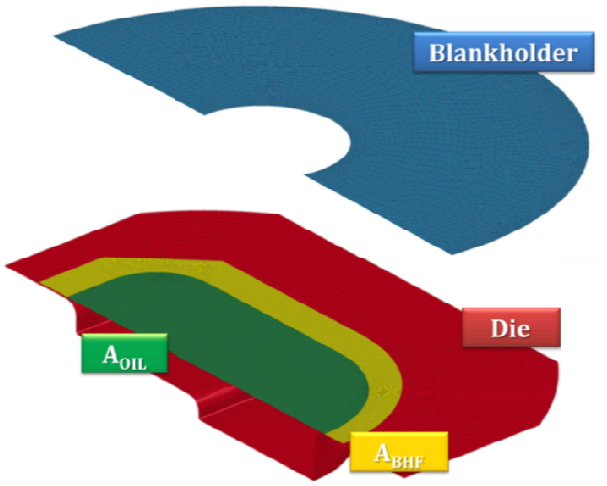

Figure 3: Parts and partitions composing the numerical model

The values of the strength coefficient (K) and the strain hardening exponent (n) are listed in Table 2 for each of the investigated temperature levels.

Table 2 Hollomon's model parameters according to temperature.

TEMPERATURE	K [MPa]	n [-]
RT	435.2	0.081
110°C	348.5	0.042
220°C	243.7	0.02

In order to take into account the anisotropy of the investigated alloy, Barlat '89 YC is considered suitable [31]. The yield function, in plane stress condition, is defined by Equation 2.

$$\Phi = a\,|K_1 + K_2|^m + a\,|K_1 - K_2|^m + c\,|2K_2|^m = 2\sigma_Y^m \quad (2)$$

where σ_Y is the yield stress, K_1 and K_2 are the stress tensor invariants, a and c are functions of the Lankford's parameters and the value of the exponent m depends on the crystallographic structure (equal to 8 for FCC alloy). Flow stress curves (along the three considered orientations) were directly implemented in the model as well as the Lankford's parameter as function of the major strain.

Computational costs were reduced both modelling only half of the blank and adopting the mass scaling technique: the absence of non-physical inertial effects was checked through the energy balance of the entire model. [32]. In order to evaluate the ruptures occurrence and the critical areas subjected to severe strain, the experimental FLCs evaluated by some of the authors in a previous work [33] were used for the post processing of results.

2.4 Response Surface Methodology and Multi - Objective Optimization

In order to evaluate the effect of the most influencing process parameters, i.e. the oil pressure, the initial and final value of the load applied by the blankholder (respectively, BHF_0 e BHF_{fin}) and the working temperature, a numerical campaign of FE simulations was scheduled according to a Central Composite Design plan. In particular, the maximum value of the oil pressure (p_{max}) was set as a percentage of the material yield stress, while the initial (BHF_0) and final (BHF_{fin}) value of the blankholder force were obtained normalizing both the initial and the final value of the blank holder pressure (i.e. the ratio between the blankholder force and the region over it acts) respectively with the yield stress and the maximum pressure; temperature was set to the same three levels used for the alloy characterization.

The adopted CCD scheme, as listed in Table 3, was characterised by investigation points at each vertex of the hyper-cube (four factors were considered), at the centre of the hyper-cube and by additional axial points (called "star points") located at a distance α (equal to 1.0 in the present work) from the design centre.

Table 3 Adopted levels of the factors investigated by the CCD plan.

Point	p_{max}/σ_y	BHp_0/σ_y	BHp_{fin}/ p_{max}	T
cube (upper value)	0.1	0.06	1.2	220
cube (lower value)	0.02	0.02	0.6	RT
axial (upper value)	0.1	0.06	1.2	220
axial (lower value)	0.02	0.02	0.6	RT
axial (centre)	0.06	0.04	0.9	110

Results from FE simulations were analysed in terms of response variables able to fully describe the process: the ratio bursting pressure over test pressure (p_{burst}/p_{max}) and the Flatness, which is defined as the ratio between the flat part of the component measured along the longitudinal direction (L_C in Figure 4) and the deepest part of the die (L_d in Figure 4).

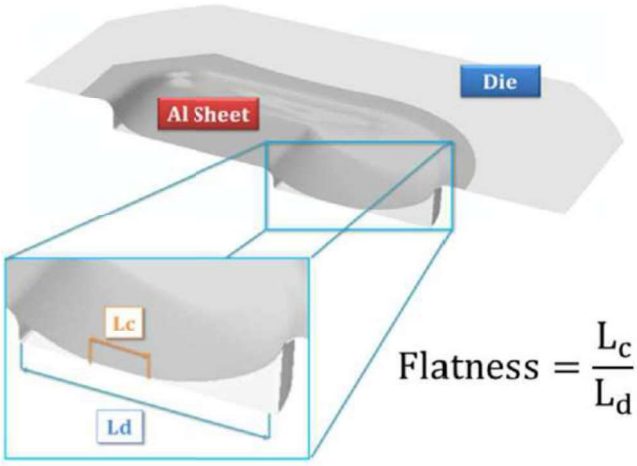

Figure 4: Definition of the output parameter *Flatness*

Simulation results, collected in terms of the above mentioned output variables, were used for creating Response Surfaces (RSs) using the commercial software modeFRONTIER. In particular, as described in the schematic workflow shown in Figure 5, for each output parameter an interpolant Radial Basis Functions (RBF) was adopted for fitting data from simulations and thus obtaining RSs able to describe the effect of the 4 input variables (I.V.) on

the Output Variables (O.V.). Such RS were thus used in the optimization procedure, aimed at maximizing both the Objective Functions (O.F. in Figure 5); in particular, a multi objective genetic algorithm was used (MOGA-II), setting a number of successive generations equal to 100 [36].

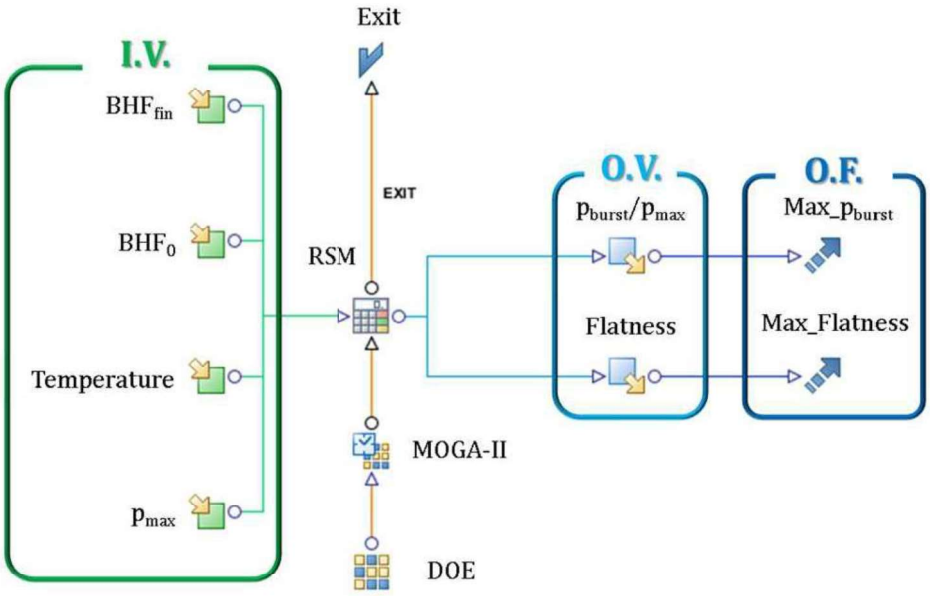

Figure 5 Overview of the resulting workflow

In order to define the RS, the whole data set was divided into two groups: the Validation Set (about 10% of the starting data set) and the Training Set (containing the remaining 90%) [34,35]. The latter was used to initially train the RS, while the Validation Set permitted to evaluate the RS performance in terms of absolute residuals. The choice for the most accurate RBF algorithm was based on: (i) the RS fitting capability in terms of minimizing the value of the Mean Leave One Out Error (MLOOE), usually optimal if less than 0.2; (ii) the small values of the absolute residuals evaluated on the Validation Set.

3. Material characterization

3.1 Mechanical characterization for the material modelling

An extensive mechanical characterization in terms of tensile tests was carried out to investigate the mechanical behaviour of the Al alloy. Flow curves in Figure 6 report the results at the explored levels of temperature when setting the strain rate to 0.0013 s^{-1}, which is representative of the strain rate condition in the sheet HF tests.

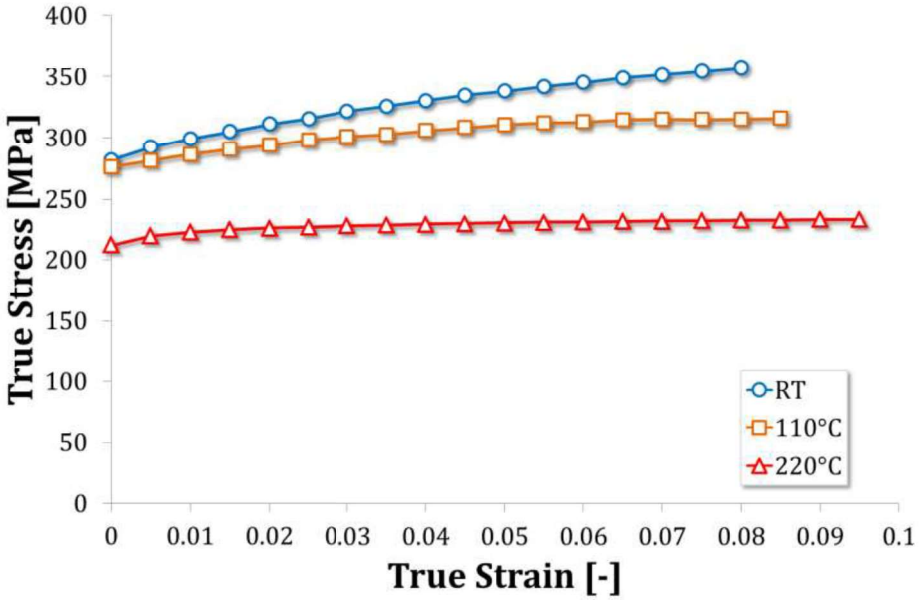

Figure 6: Flow stress curves according to temperature

The difference in the strength properties when considering the rolling, the transverse and the intermediate directions was taken into account evaluating the anisotropic behaviour of the material in terms of Lankford's parameters (R_0, R_{45} R_{90}): strains along both the longitudinal and transversal directions (respectively major and minor strain) were monitored in three different points up to the onset of necking (dashed line in Figure 7a).

The R-values could be thus calculated as the ratio between the minor strain and the thickness strain. The evolution of the normal anisotropy as a function of the major strain is reported in Figure 7b.

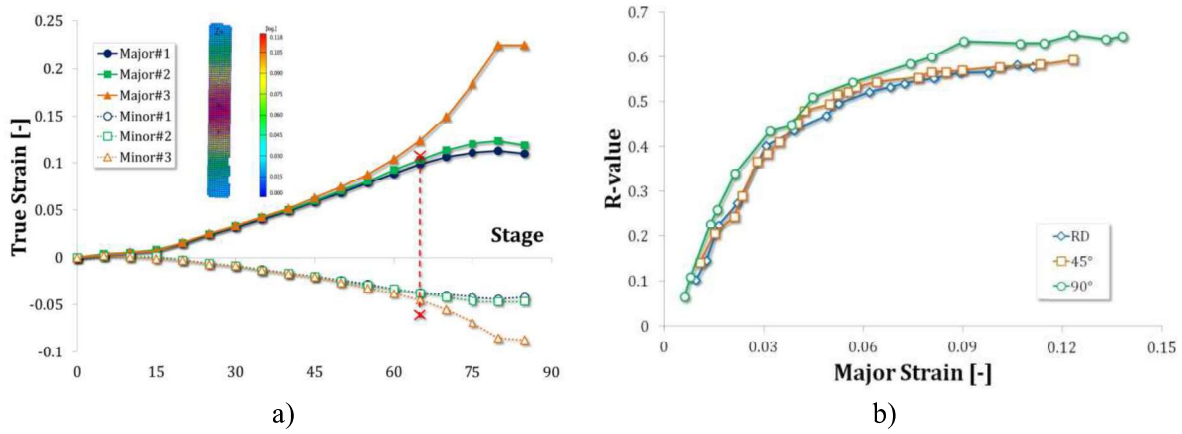

Figure 7: (a) Principal stain evolution during tensile tests; (b) normal anisotropy according to major strain

3.2 Warm Hydroforming tests for the CoF evaluation

In the WHF process, interactions between parts in contact result to be an important aspect: the sheet, for example, is in contact with both the die and the Blank Holder; the CoF thus plays a relevant role in the distribution of strains during the whole process.

In order to obtain an accurate evaluation of the CoF value, an inverse analysis was performed comparing the experimental thickness distribution acquired by means of the DIC system along the longitudinal path with the correspondent numerical one: the CoF value was evaluated as the one able to determine the best fitting of the two thickness distributions. In addition, the above mentioned procedure was carried out at each of the investigated levels of temperature in order to take into account any variation of the rheological properties of the oil when changing the working temperature.

Numerical thickness strains along the longitudinal path have been plotted in Figure 8(a and b) together with the correspondent experimental ones (experimental plots are not continuous

because of the lack of data in the central region due to the loss of the painting caused by the contact with the die).

Results from the inverse analysis are obviously characterised by a good overlapping between numerical and experimental data, being the difference of thickness strains almost negligible both in the case of the isotropic (Figure 8a) and the anisotropic YC (Figure 8b).

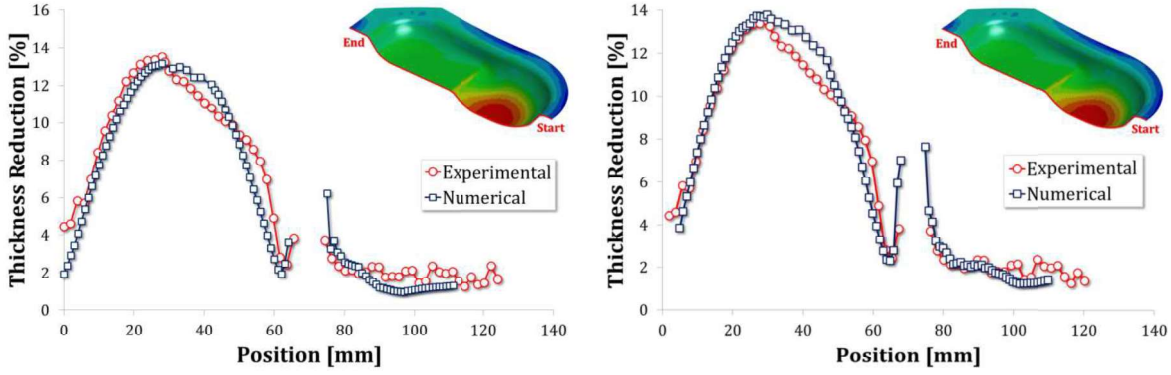

a) b)

Figure 8: Thickness reduction comparisons (T=220°C, BHF=76-131kN, p=10-84 bar): a) isotropic modelling, b) anisotropic modelling

Results of the inverse analysis, according to temperature and YC, are resumed in Table 4.

Table 4 Values of the Coefficient of friction according to temperature and yield criteria.

TEMPERATURE	CoF (Von Mises)	CoF (Barlat '89)
20°C	0.095	0.055
110°C	0.068	0.055
220°C	0.08	0.055

4. Results and discussion

4.2 Numerical evaluation of the working range according to yield condition

According to the CCD scheme, a total number of 25 simulations were run for each of the two models implementing the different yield criteria. Figure 9 contains the contour plots of the

RSs created using results (in terms of Flatness and p_{burst}/p_{max}) from the model implementing the Barlat YC (Figure 9a and Figure 9b) and from the model implementing the isotropic YC (Figure 9c and Figure 9d).

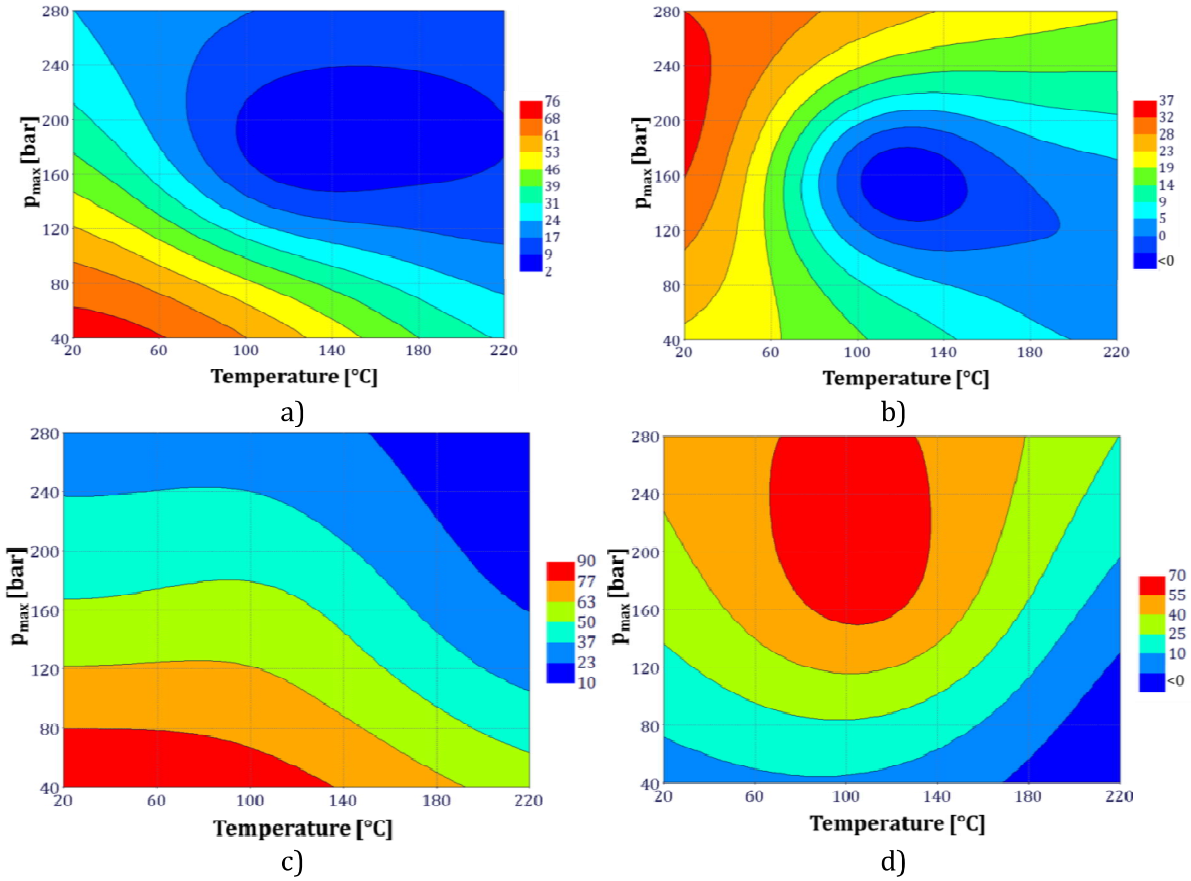

Figure 9: Contour plots of the RSs created using data from FE simulations: a) p_{burst}/p_{max} (anisotropic YC), b) Flatness (anisotropic YC), c) pburst/pmax (isotropic YC), d) Flatness (isotropic YC).

Comparing the contour plots in Figure 9 it may be noted that the choice of the YC has an appreciable influence on the final results: lower values of the temperature seems to be preferable in order to produce a more formed component (larger Flatness values) if the anisotropy is accounted for.

On the contrary, from FE simulations implementing an isotropic behaviour result a shifting of the region of large Flatness values toward higher temperatures. Such a result is more clearly presented in Figure 10, where the extension of the flat region of the deepest part has been plotted for the simulations carried out using the anisotropic YC and the Von Mises one.

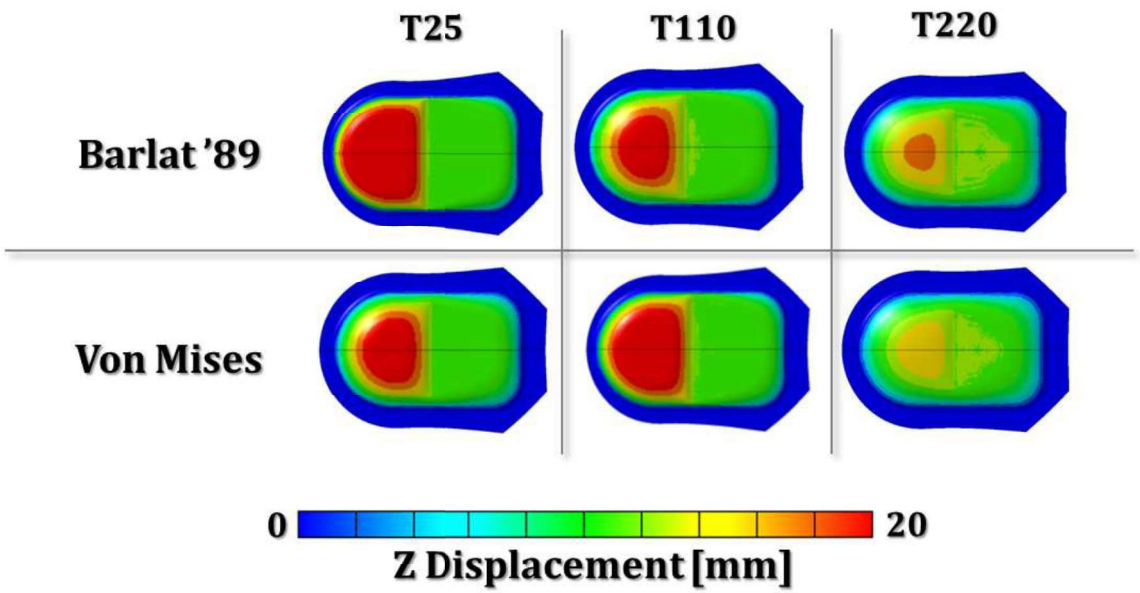

Figure 10: Extension of the flat region of the deepest part according to temperature using both YC

In order to evaluate the working conditions able to maximise both the response variables, two different optimization procedures were carried out, using both the FE models and thus investigating the effect of the YC on the optimization results.

In Figure 11 results from the optimization procedure are summarised in terms of values assumed by the two response parameter when changing the factors.

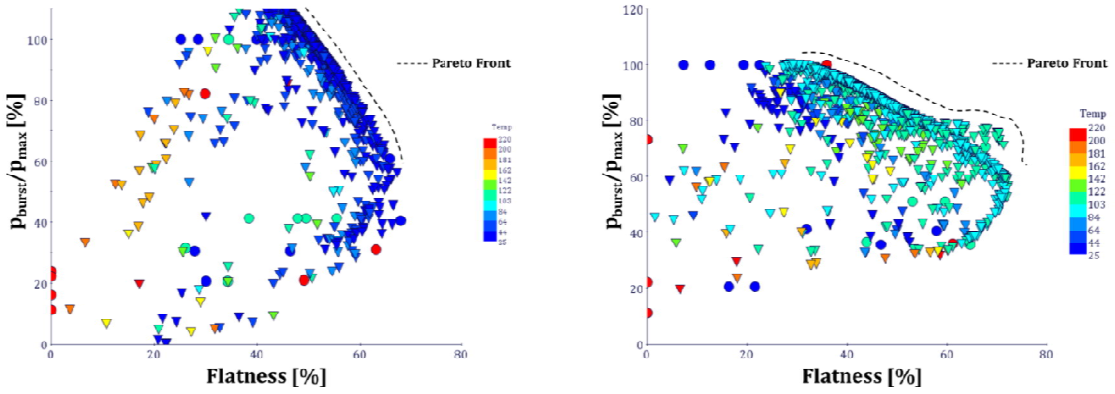

a) b)

Figure 11: Results from the optimization procedure: a) optimal designs (anisotropic YC); b) Pareto Front (anisotropic YC).

Results in Figure 11 show that, if anisotropy is neglected, optimal working conditions can be found when temperature is set at an average value (ranging from 80 to 110°C), while room temperature is the optimal temperature value if the anisotropic YC is used.

4.3 Hydroforming tests for the validation of virtual designs

In order to validate numerical results and, thus, to understand which yield criterion is most able to catch the real material behaviour and thus to furnish the most accurate / robust results, a set of experimental WHF tests was designed starting from the CCD plan adopted for the numerical analysis.

The incremental space filler (ISF) algorithm was adopted to insert new combinations of the factors (I.V.) able to fill the original design space uniformly. As shown in Figure 12, such an algorithm is useful to generate an uniform distribution of designs in the input space: it considers the existing points in the database and adds sequentially new points where the minimum distance from the existing points is maximized [34].

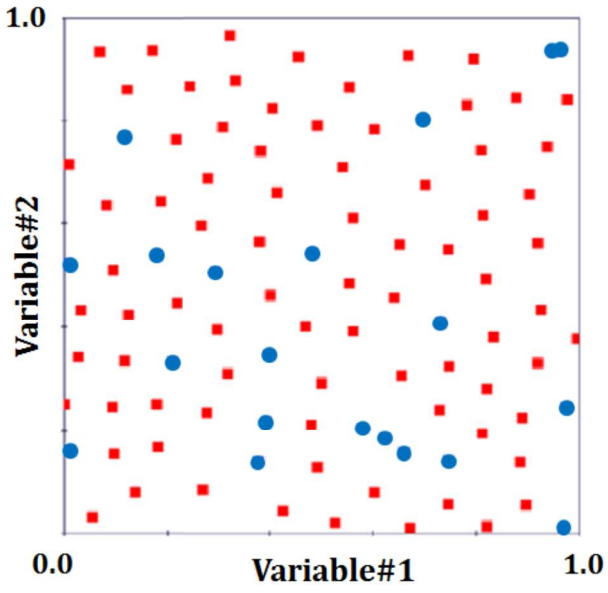

Figure 12 ISF: New points (red squares) are added to existing point in database (blue circles) in order to fill the space in a uniform way.

Experimental hydroforming tests were also analysed in terms of Flatness and p_{burst}/p_{max}, the same response variables used for data from numerical simulations. In Figure 13 tests conducted at different temperatures when setting the same value of the maximum pressure (p_{max}/σ_{y0} = 0.05) have been presented in terms of extension of the deepest region (20mm depth), that is the region in contact with the deepest part of the die.

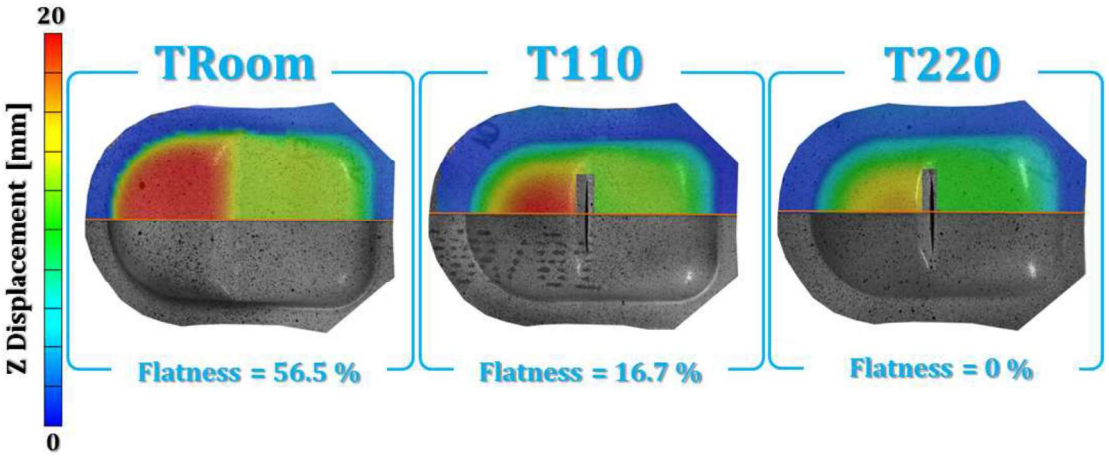

Figure 13 Experimental acquisitions of deformed sheet at three different levels of temperature using the DIC system

It can be noted that, comparing the regions highlighted in red, low temperature is beneficial for the formability of the component. If the working temperature increased, not only the extension of the flat region decreased, but rupture also occurred.

The above mentioned data (this time from experiments) were used to create the RSs of both the adopted response variables and thus to carry out the optimization procedure. Results have been presented in Figure 14a, which shows the Pareto containing the optimal virtual designs. It may be noted that experiments indicated as optimal the working conditions characterised by low temperature values, confirming the accuracy of the optimization results obtained by the FE model implementing the anisotropic YC.

Finally in Figure 14b all Pareto fronts (both the numerical ones and the experimental one) have been compared.

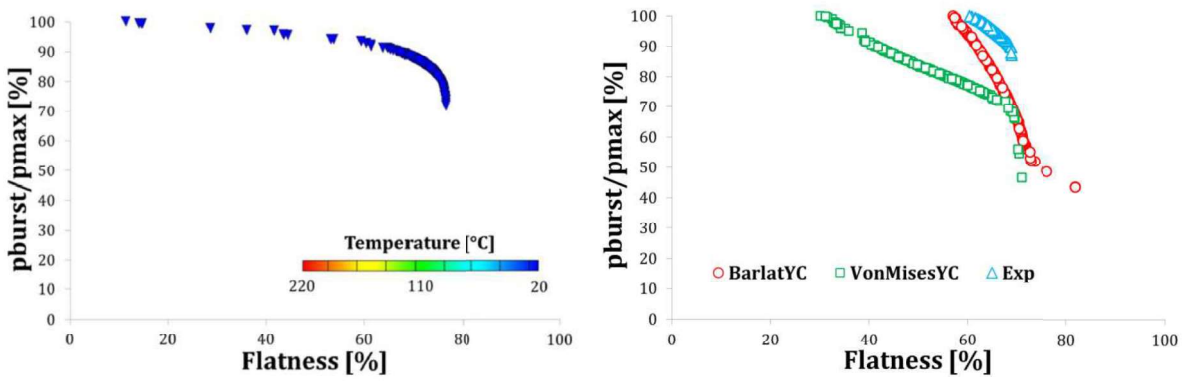

a) b)

Figure 14 a) Pareto Front, b) comparison of the obtained Pareto Fronts

It may be noted that the Pareto front obtained starting from experimental results (only the portion of the Pareto front characterized by the best Flatness values was considered) agrees well with the one obtained using the FE model implementing the Barlat89 YC.

Conclusions

Sheet Hydroforming confirmed to be a stamping process suitable for forming light alloys and highly able to easily create components characterised by complex shapes.

The proposed numerical models, even if simple, revealed to be able to accurately reproduce the strain field distribution and using any Yield Conditions if properly tuned (i.e. calibrating the friction coefficient according to the level of temperature by an inverse analysis approach).

But great attention has to be paid to the material modelling: according to the Yield Condition (in this work the isotropic formulation by Von Mises and the anisotropic model by Barlat '89 were considered) the numerical model gives back different results when changing the process parameters (Blank Holder Force, oil pressure, Temperature).

The multi-objective optimization carried out in the present research highlighted that the shape of the Pareto front (the locus of the virtual optimal designs) strongly changes according to the Yield Criterion used for modelling the material plasticity: a sound and, at the same time,

well-formed component can be obtained at room temperature when the anisotropic behaviour is taken into account, while the adoption of an isotropic formulation shifts the operative window towards warm temperatures.

Experimental tests conducted to validate the results of the numerical optimization confirmed the robustness of the FE model implementing the anisotropic Yielding and demonstrated that the tuning procedure simply based on the best fitting of numerical and experimental data by changing the friction coefficient is poor and not able to catch the real material stamping behaviour.

Acknowledgement

The authors wish to thank APULIA Region for financing the present research activity through the funding of the regional labs network "TRASFORMA".

References

[1]. Schultz RA. "Aluminum for light vehicles – an objective look at the next ten to twenty years". 14th International Aluminum Conference, Montreal, Canada (Ducker Research), September 15, 1999.

[2]. Hirsch J. "Aluminium in Innovative Light-Weight car design". Mat Trans 52 (2011): 818-24.

[3]. Miller W.S., Zhuang L., Bottema J., Wittebrood A.J., De Smet P., Haszler A., Vieregge A. "Recent development in aluminium alloys for the automotive industry". Mater Sci Eng A280 (2000):37-49.

[4]. Novotny S, Geiger M. "Process design for hydroforming of lightweight metal sheets at elevated temperatures". J Mater Process Technol 38 (2003):594-9.

[5]. D. Li, A. Ghosh, Tensile deformation behavior of aluminum alloys at warm forming temperatures, Mater Sci Eng A 352 (2003): 279–86.

[6]. N. Abedrabbo, F. Pourboghrat, F. Carsley, Forming of aluminum alloys at elevated temperatures. Part 1. Material characterization, Int J Plasticity 22 (2006): 314–41.

[7]. T. Naka, G. Torikai, R. Hino, F. Yoshida "The effects of temperature and forming speed on the forming limit diagram for type 5083 aluminum–magnesium alloy sheet", J Mater Process Technol 113 (2001): 648-53.

[8]. Mahabunphachai S, Koç M. "Investigations on the forming of aluminum 5052 and 6061 sheet alloys at warm temperatures". Mater Design 31 (2010):2422-34.

[9]. Lucke HU, Hartl Ch, Abbey T. “Hydroforming”. J Mater Process Technol 115 (2001): 87-91.
[10]. Siegert K, Häussermann M, Lösch B, Rieger R. “Recent developments in hydroforming technology”. J Mater Process Technol 98 (2000): 251-58.
[11]. Hein P, Vollertsen F. ““Hydroforming of sheet metal pairs”. J Mater Process Technol 87 (1999):154-64.
[12].
[13]. Lang LH, Wang ZR, Kang DC, Yuan SJ, Zhang SH, Danckert J, Nielsen KB. “Hydroforming highlights: sheet hydroforming and tube hydroforming”. J Mater Process Technol 151 (2004):165-77.
[14]. Kim BJ, Van Tyne CJ, Lee MY, Moon YH. “Finite element analysis and experimental confirmation of warm hydroforming process for aluminium alloy”. J Mater Process Technol 187-188 (2007): 296-99.
[15]. Planack M, Vollersten F, Woitschig J. “Analysis, finite element simulation and experimental investigation of friction in tube hydroforming”. J Mater Process Technol 170 (2005):220-28.
[16]. Vollersten F, Plancak M. “On possibilities for the determination of the coefficient of friction in hydroforming of tubes”. J Mater Process Technol 125-126 (2002): 412-20.
[17]. Korkolis YP, Kyriakides S. “Hydroforming of anisotropic aluminum tubes: Part II analysis”. Int J Mech Sci 53 (2011): 83-90.
[18]. Hill R. “The mathematical theory of plasticity” Clarendon Press, New York: Oxford University Press (1983).
[19]. Mattiasson K, Sigvant M. “An evaluation of some recent yield criteria for industrial simulations of sheet forming processes”. Int J Mech Sci 50 (2008): 774-87.
[20]. Banabic D, Barlat F, Cazacu O, Kuwabara T. “Advances in anisotropy and formability”. Int J Mater Form 3 (2010) 165-189.
[21]. Comsa S, Cosovici G, Jurco P, Paraianu L, Banabic D. “Simulation of the hydroforming process using a new orthotropic YC”. J Mater Process Technol 157-158 (2004): 67-74.
[22]. Fann KJ, Hsiao PY. “Optimization of loading conditions for tube hydroforming”. J Mater Process Technol 140 (2003): 520-24.
[23]. Yang JB, Jeon BH, Oh SI. “Design sensitivity analysis and optimization of the hydroforming process”. J Mater Process Technol 113 (2001): 666-72.
[24]. Abedrabbo N, Worswick M, Mayer R, van Riemsdijkc I. “Optimization methods for the tube hydroforming process applied to advanced high-strength steels with experimental verification”. J Mater Process Technol 209 (2009): 110-23.
[25]. Castro CF, António CAC, Sousa LC. “Optimisation of shape and process parameters in metal forging using genetic algorithms”. J Mater Process Technol 146 (2004): 356-64.
[26]. Mirzaali M, Seyedkashi SMH, Liaghat GH, Moslemi Naeini H, G Shojaee K, Moon YH. “Application of simulated annealing method to pressure and force loading optimization in tube hydroforming process”. Int J Mech Sci 55 (2012): 78-84.
[27]. Jansson T, Andersson A, Nilsson L “Optimization of draw-in for an automotive sheet metal part – an evaluation using surrogate models and response surfaces”. J Mater Process Technol 159 (2005): 426-34.

[28]. Naceur H, Guo YQ, Ben-Elechi S. "Response Surface Methodology for design of sheet forming parameters to control springback effect". Comput Struct 84 (2006): 1651-63.
[29]. LS-DYNA Theory Manual, Livermore Software Technology Corporation, March 2006.
[30]. LS-DYNA Keyword User's Manual Vol.2 Vers. R7.0, Livermore Software Technology Corporation, Feb.2013.
[31]. Barlat F, Lian K. "Plastic behaviour and stretchability of sheet metal. Part I: A yield function for orthotropic sheets under plane stress condition". Int J Plasticity 5 (1989): 51-66.
[32]. LS-DYNA Keyword User's Manual Vol.1 Vers. R7.0, Livermore Software Technology Corporation, Feb.2013.
[33]. Palumbo G, Piccininni A. "Numerical-experimental investigations on the manufacturing of an aluminium bipolar plate for the proton exchange membrane fuel cells by warm hydroforming", Int J Adv Manuf Tech 69 (2013): 731-42.
[34]. modeFRONTIER (v. 4.5.3) User's Manual, 2014.
[35]. Buhmann MD, Martin D. "Radial Basis Functions: Theory and Implementations". Cambridge University Press, UK, 2003.
[36]. Deb K. "Multi-Objective Genetic Algorithms: Problems Difficulties and Construction of Test Problems". Evol Comput 7 (1999): 205-30

Table 01

Si %	Fe %	Cu %	Mn %	Mg %	Cr %	Zn %	Ti %
0.67	0.42	0.23	0.10	0.92	0.18	0.04	0.07

Table 02

TEMPERATURE	K [MPa]	n [-]
RT	435.2	0.081
110°C	348.5	0.042
220°C	243.7	0.02

Table 03

Point	p_{max}/σ_y	BHp_0/σ_y	BHp_{fin}/ p_{max}	T
cube (upper value)	0.1	0.06	1.2	220
cube (lower value)	0.02	0.02	0.6	RT
axial (upper value)	0.1	0.06	1.2	220
axial (lower value)	0.02	0.02	0.6	RT
axial (center)	0.06	0.04	0.9	110

Table 04

TEMPERATURE	CoF (Von Mises)	CoF (Barlat ’89)
RT	0.095	0.055
110°C	0.068	0.055
220°C	0.08	0.055

Figure 1a

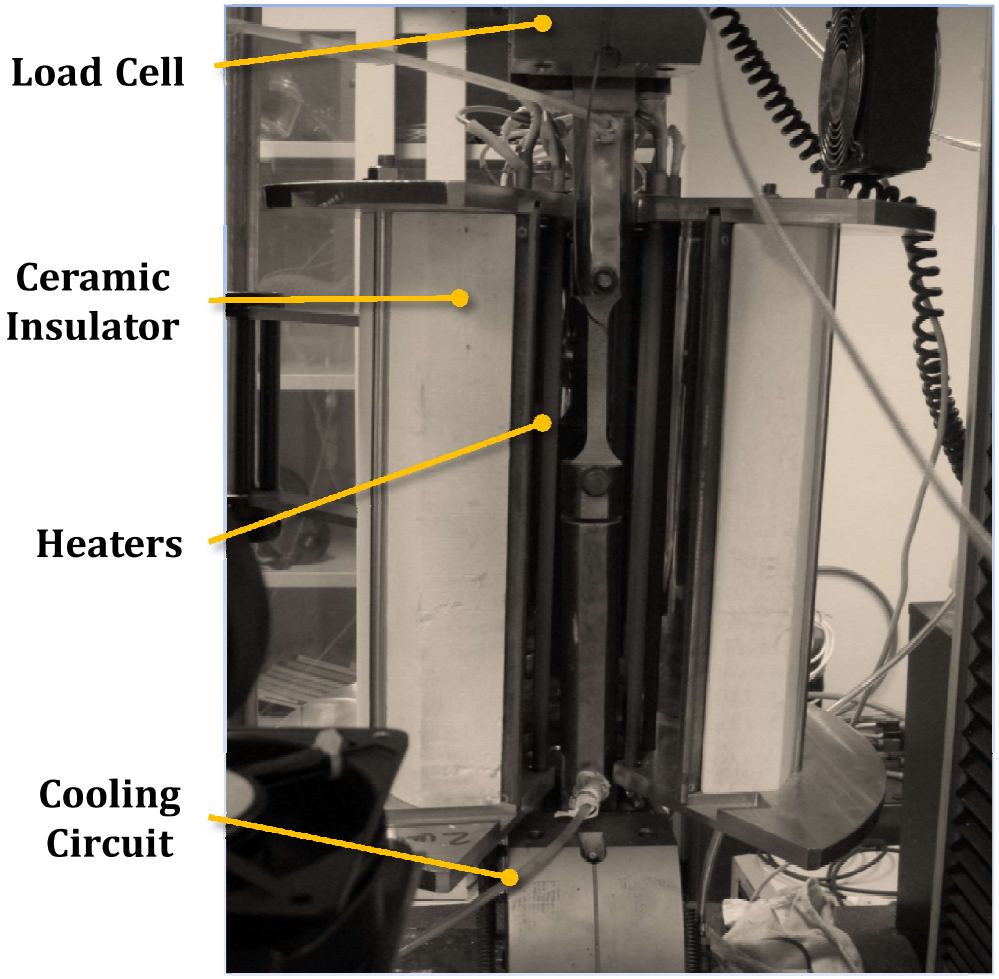

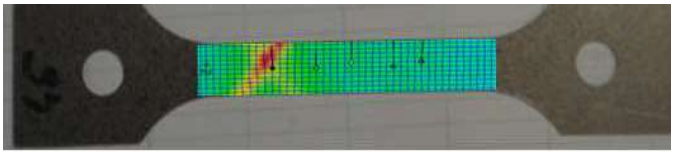

Figure 1b

Figure 2a

Figure 2b

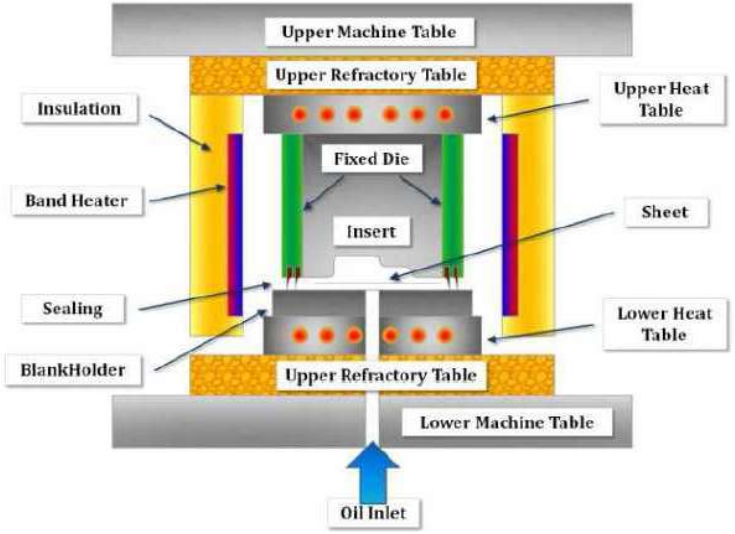
Upper Machine Table
Upper Refractory Table
Upper Heat Table
Insulation
Fixed Die
Band Heater
Sheet
Insert
Sealing
Lower Heat Table
BlankHolder
Upper Refractory Table
Lower Machine Table
Oil Inlet

Figure 2c

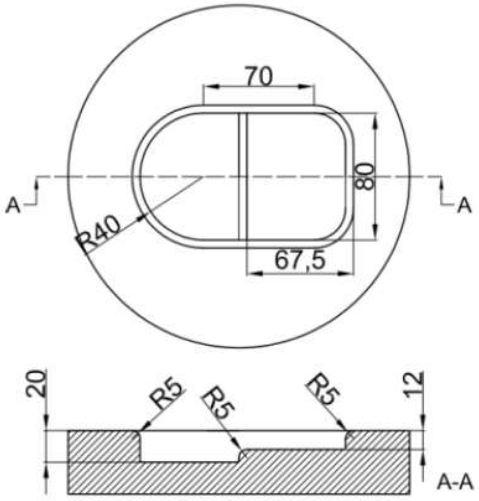

Figure 3

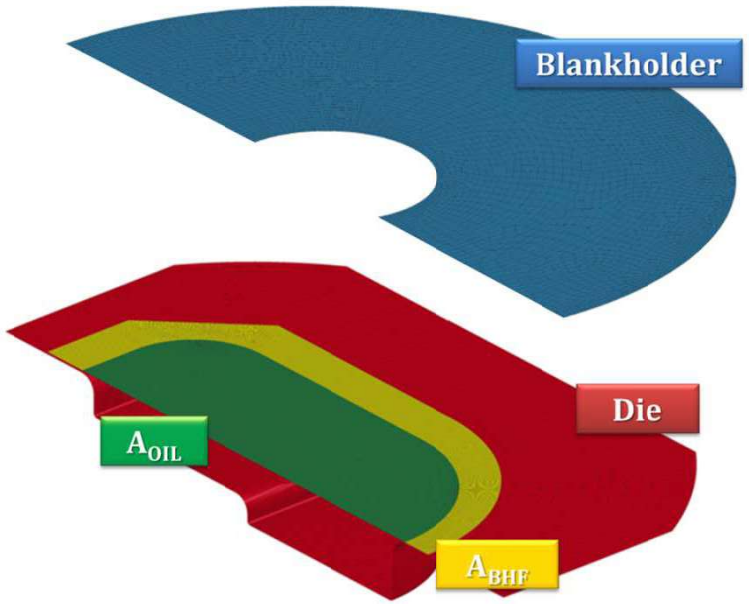

Figure 4

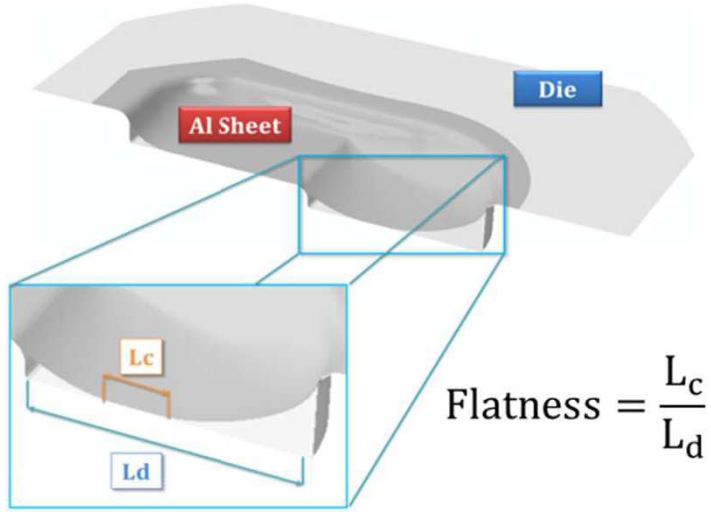

Figure 5

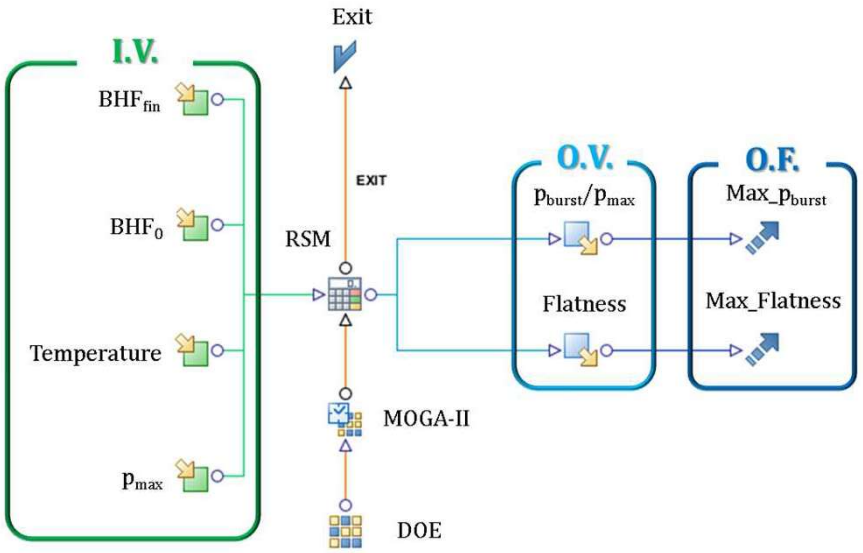
Exit
I.V.
BHF_{fin}
BHF_0
Temperature
p_{max}
EXIT
RSM
MOGA-II
DOE
O.V.
p_{burst}/p_{max}
Flatness
O.F.
Max_p_{burst}
Max_Flatness

Figure 6

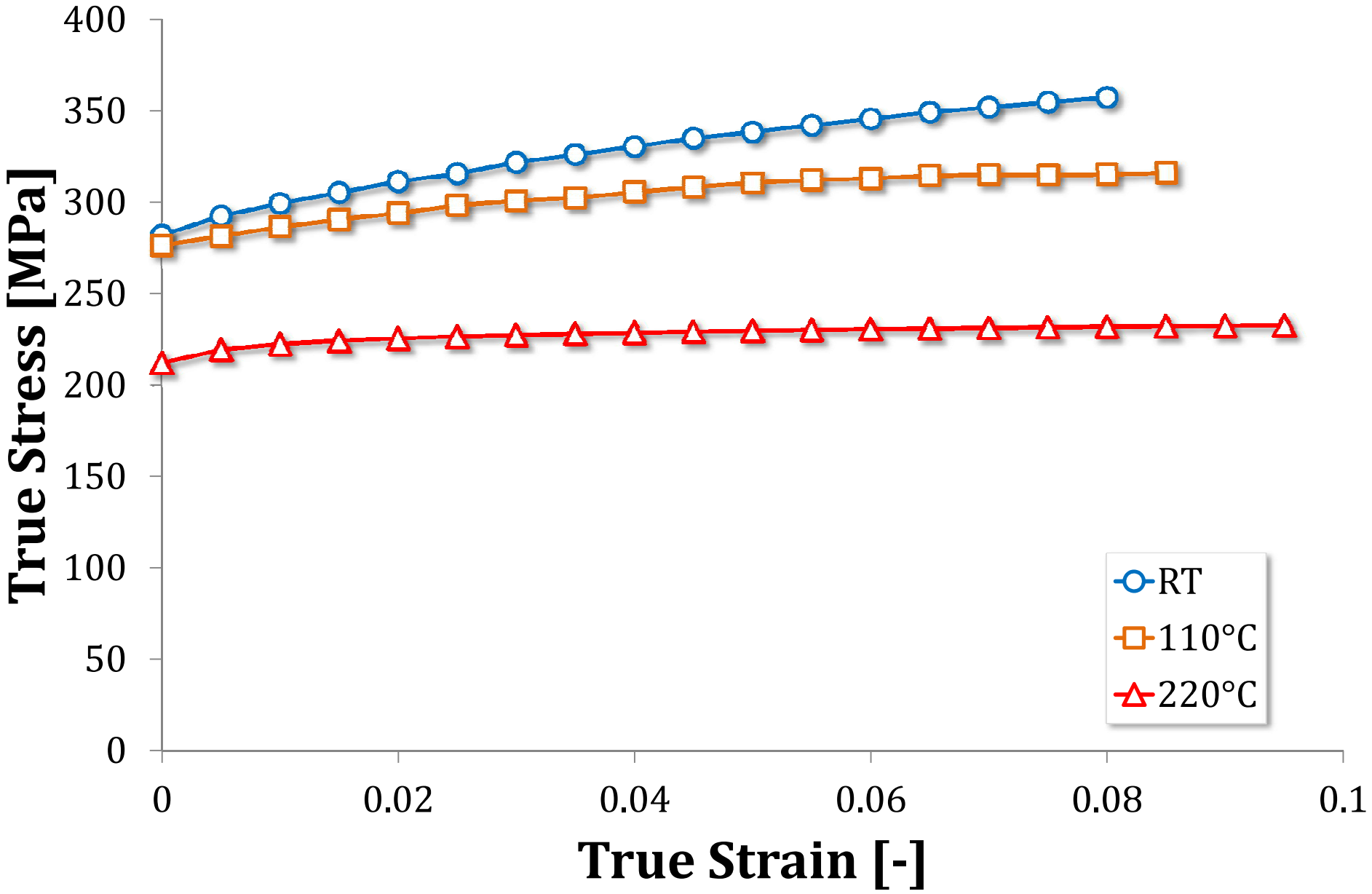
400
350
300
250
200
150
100
50
0
True Stress [MPa]
0
0.02
0.04
0.06
0.08
0.1
True Strain [-]
RT
110°C
220°C

Figure 7a

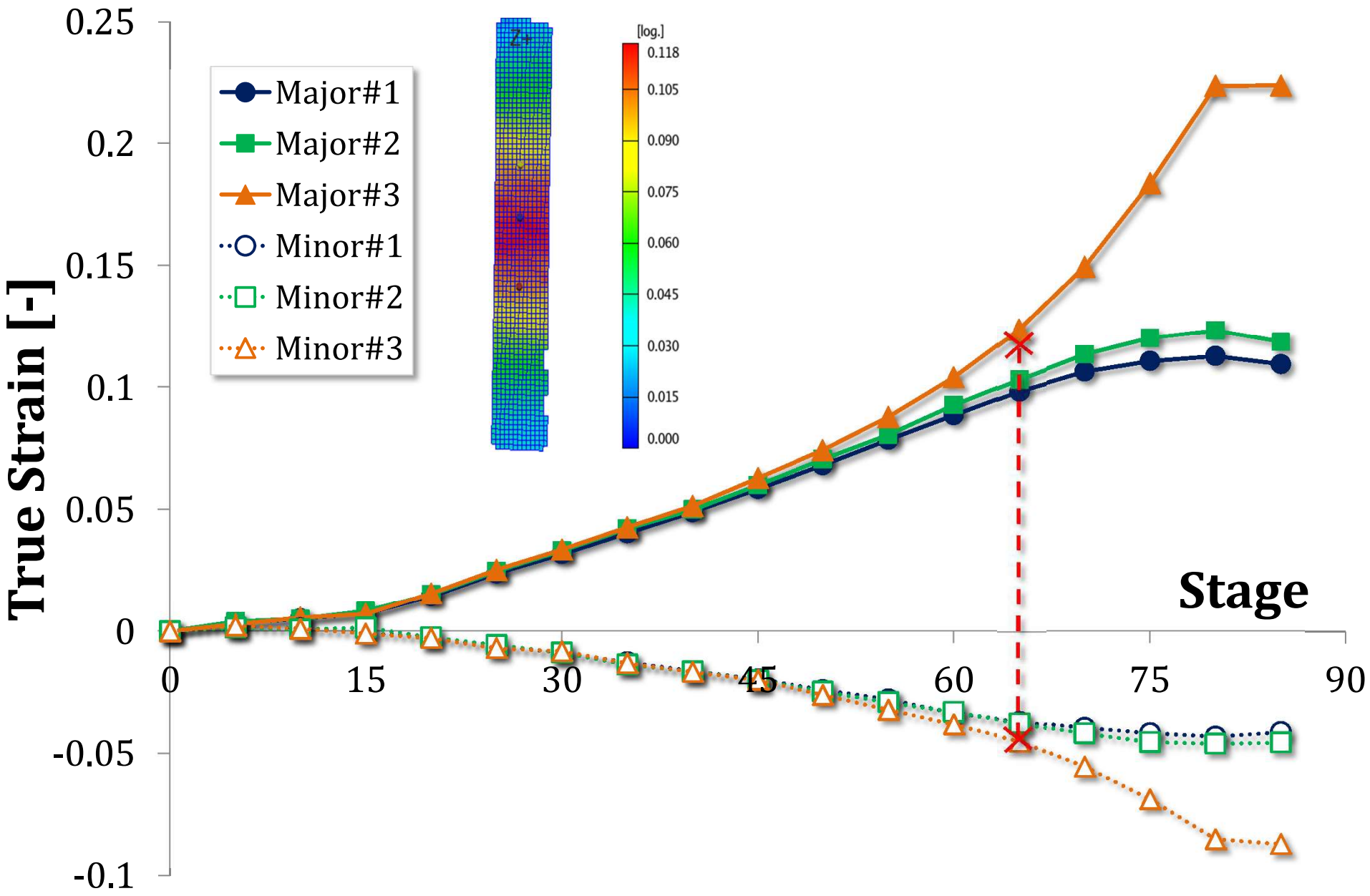
True Strain [-]
0.25
0.2
0.15
0.1
0.05
0
-0.05
-0.1
0
15
30
45
60
75
90
Stage
Major#1
Major#2
Major#3
Minor#1
Minor#2
Minor#3
[log.]
0.118
0.105
0.090
0.075
0.060
0.045
0.030
0.015
0.000

Figure 7b

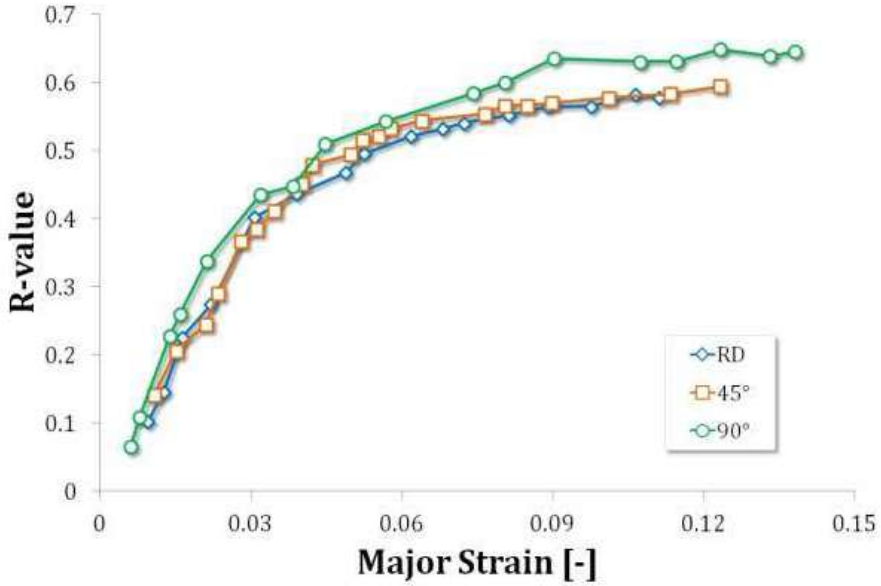
0.7
0.6
0.5
0.4
0.3
0.2
0.1
0
R-value
0
0.03
0.06
0.09
0.12
0.15
Major Strain [-]
RD
45°
90°

Figure 8a

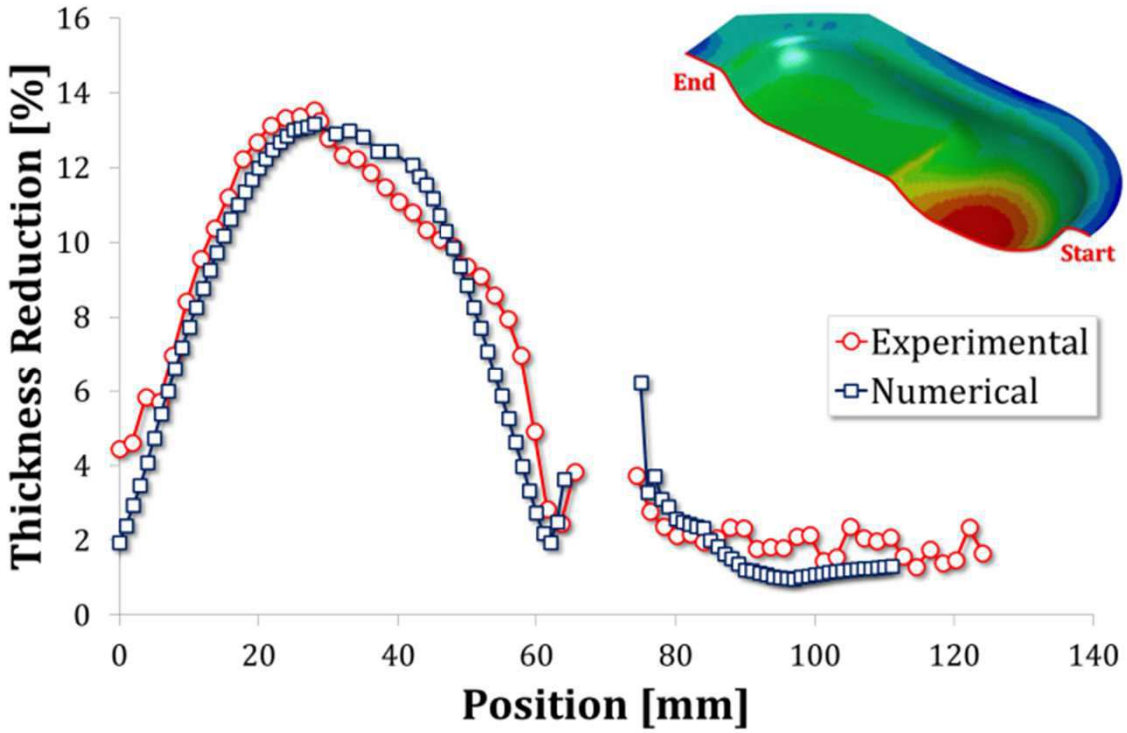
Thickness Reduction [%]
16
14
12
10
8
6
4
2
0
0
20
40
60
80
100
120
140
Position [mm]
End
Start
Experimental
Numerical

Figure 8b

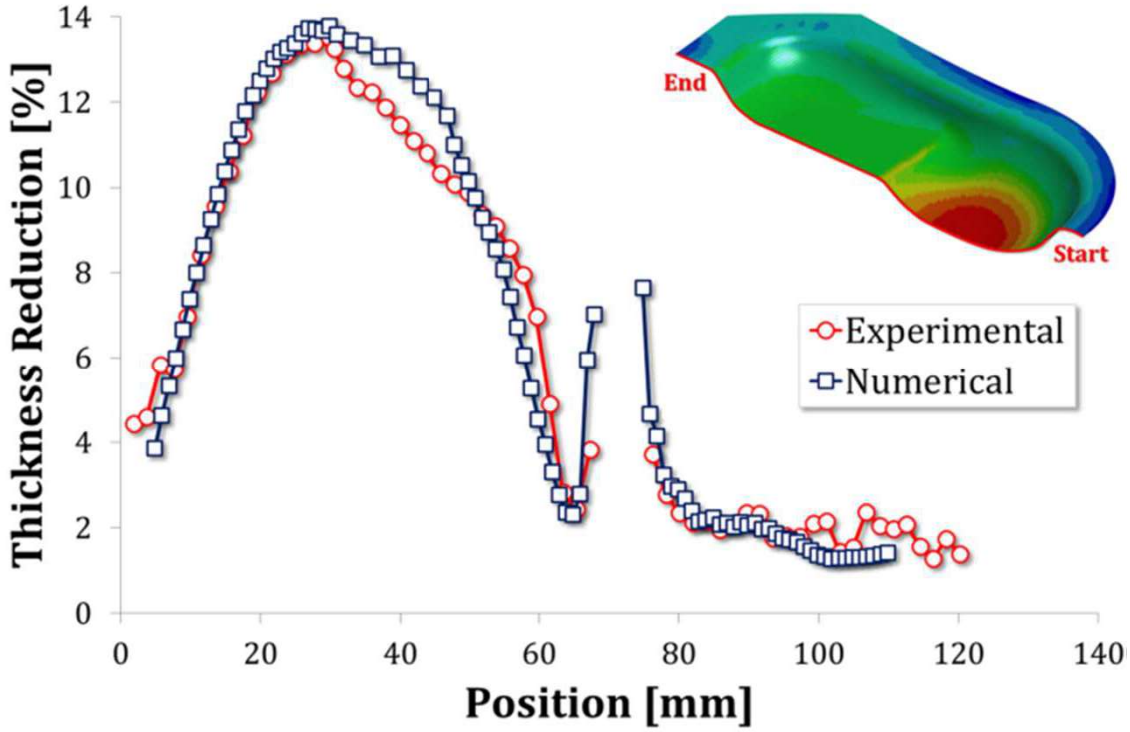
Thickness Reduction [%]
0
2
4
6
8
10
12
14
0
20
40
60
80
100
120
140
Position [mm]
End
Start
Experimental
Numerical

Figure 9a

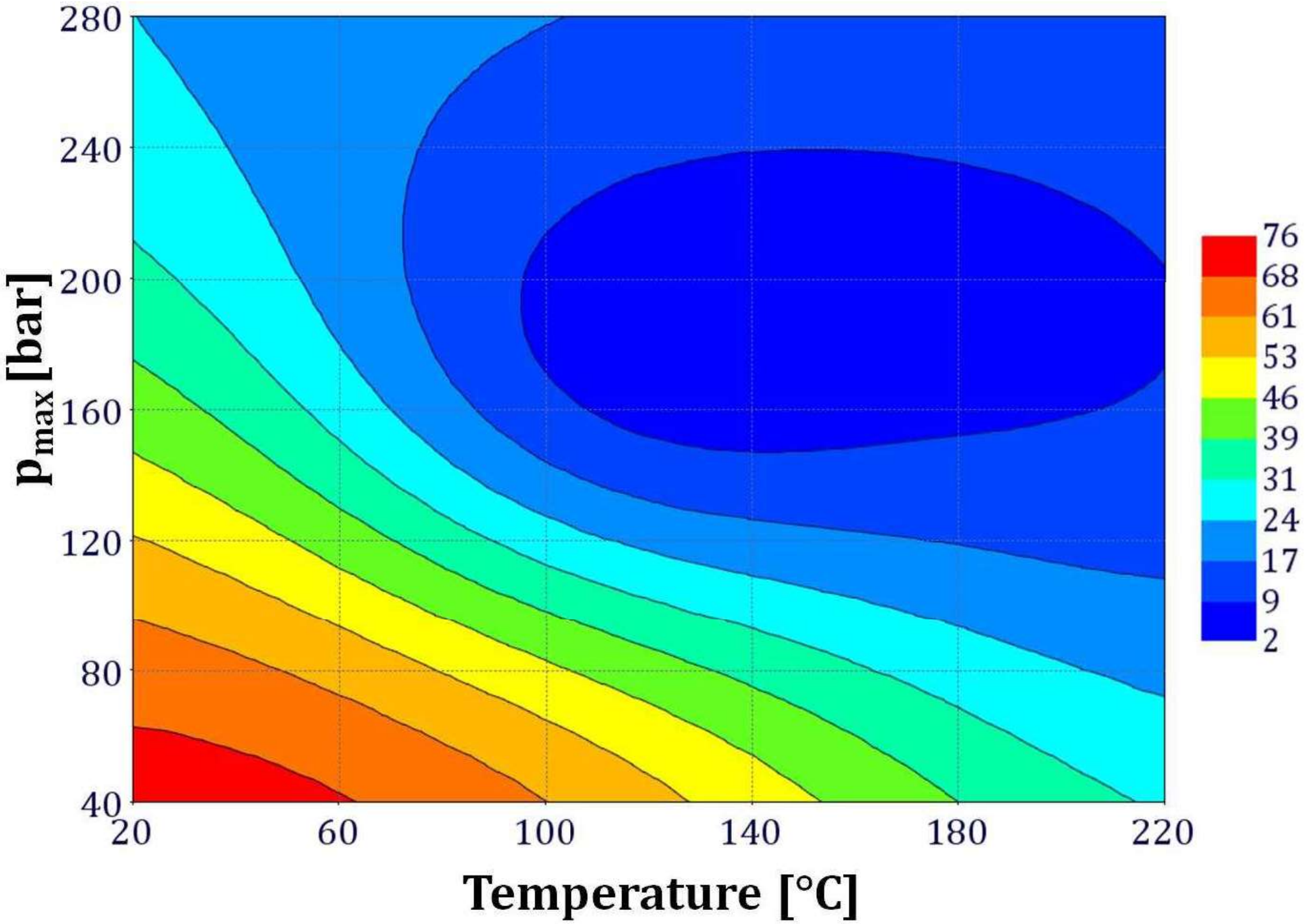
280
240
200
160
120
80
40
p_{max} [bar]
20
60
100
140
180
220
Temperature [°C]
76
68
61
53
46
39
31
24
17
9
2

Figure 9b

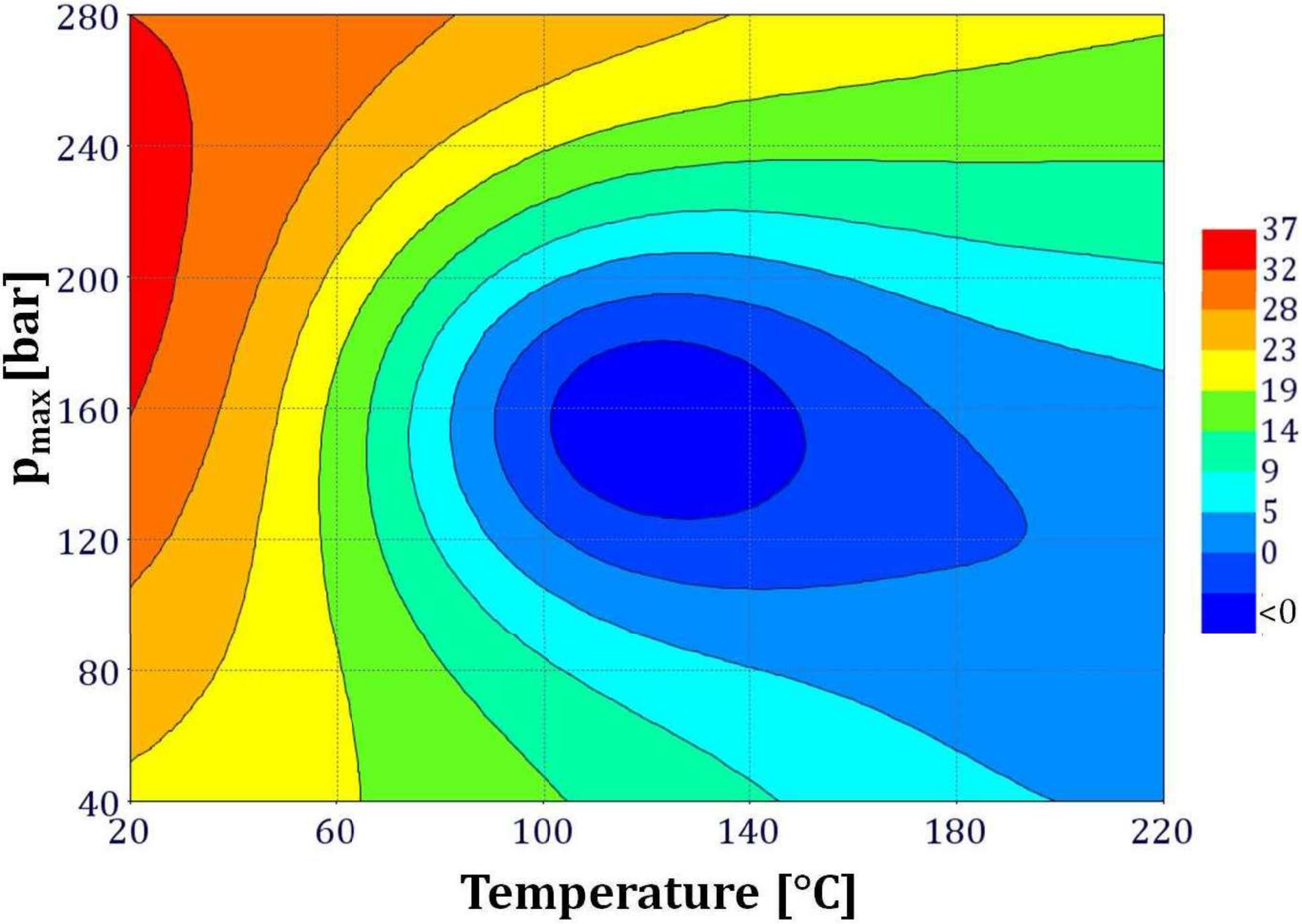
280
240
200
160
120
80
40
p_{max} [bar]
20
60
100
140
180
220
Temperature [°C]
37
32
28
23
19
14
9
5
0
<0

Figure 9c

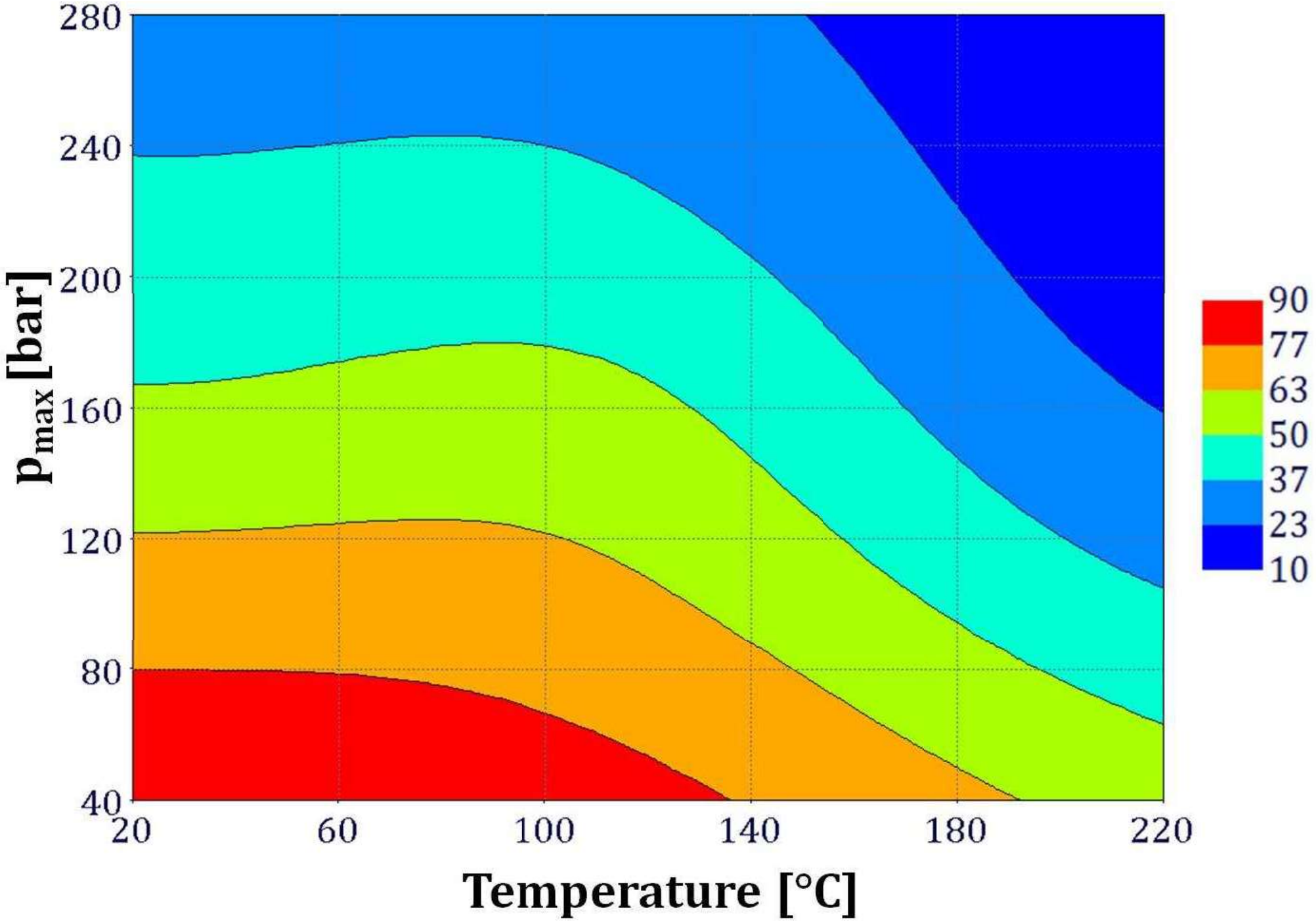
280
240
200
160
120
80
40
p_{max} [bar]
20
60
100
140
180
220
Temperature [°C]
90
77
63
50
37
23
10

Figure 9d

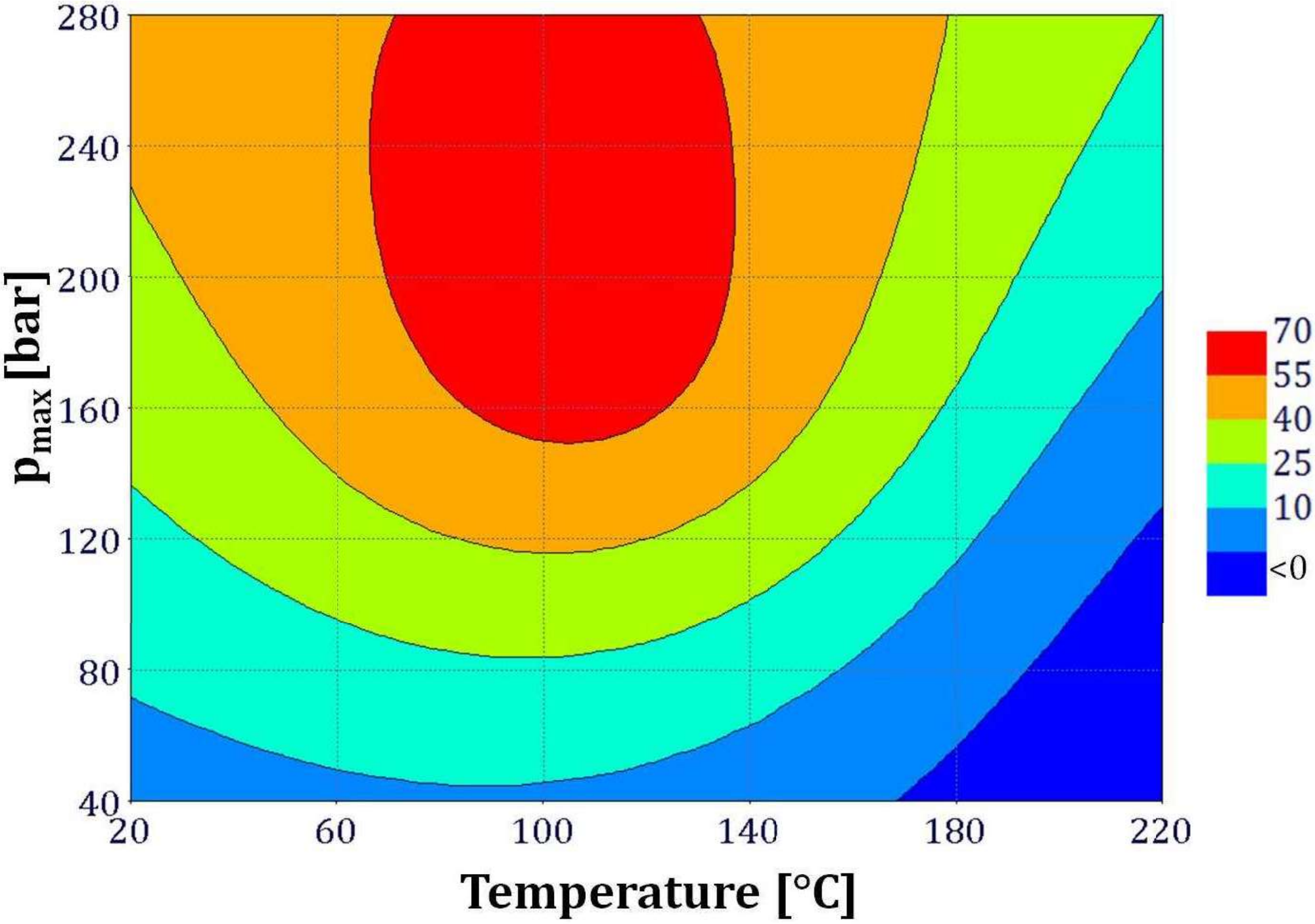
280
240
200
160
120
80
40
p_{max} [bar]
20
60
100
140
180
220
Temperature [°C]
70
55
40
25
10
<0

Figure 10

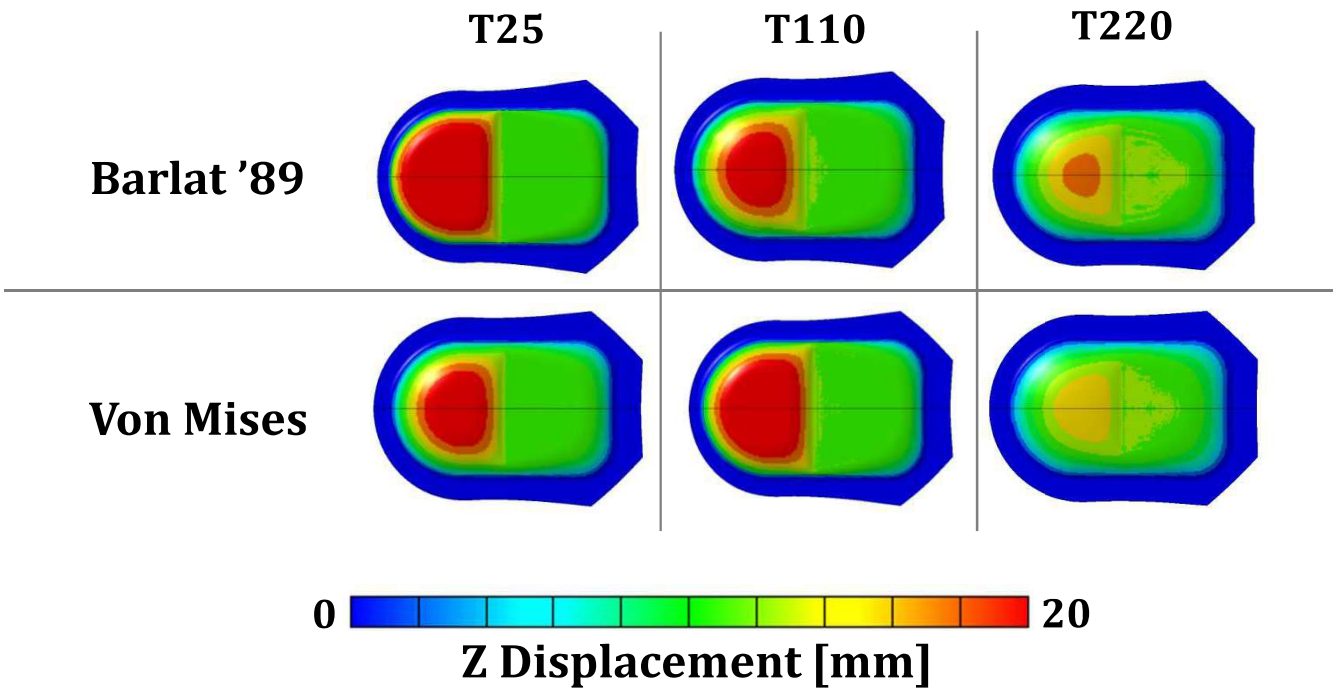

Figure 11a

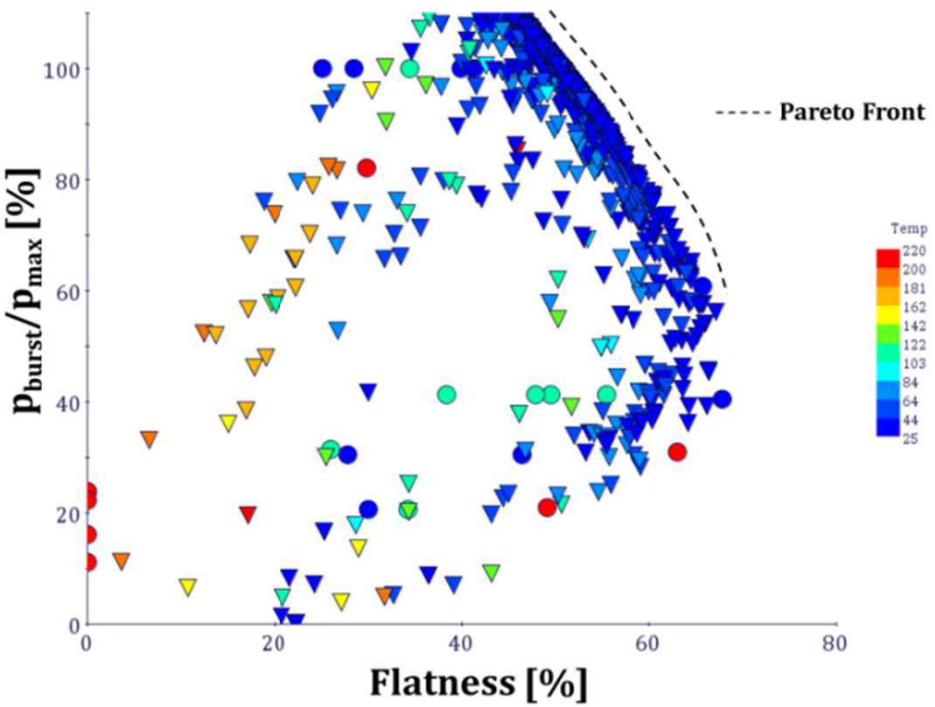
Pareto Front
Temp
220
200
181
162
142
122
103
84
64
44
25
p_{burst}/p_{max} [%]
Flatness [%]
0
20
40
60
80
100

Figure 11b

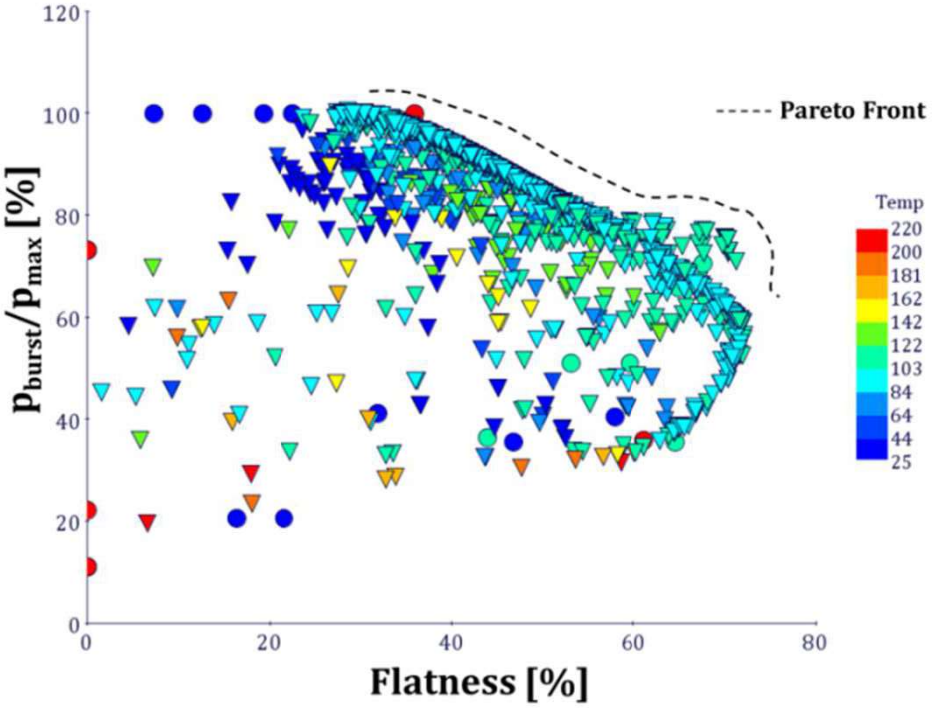
120
100
80
60
40
20
0
0
20
40
60
80
p_{burst}/p_{max} [%]
Flatness [%]
Pareto Front
Temp
220
200
181
162
142
122
103
84
64
44
25

Figure 12

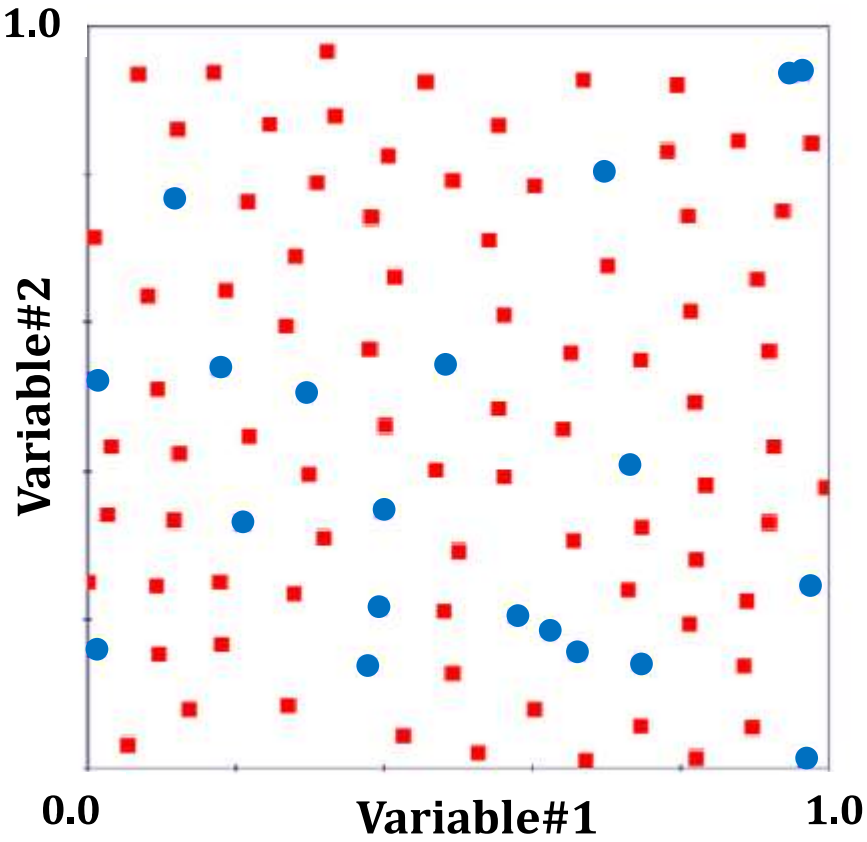

Figure 13

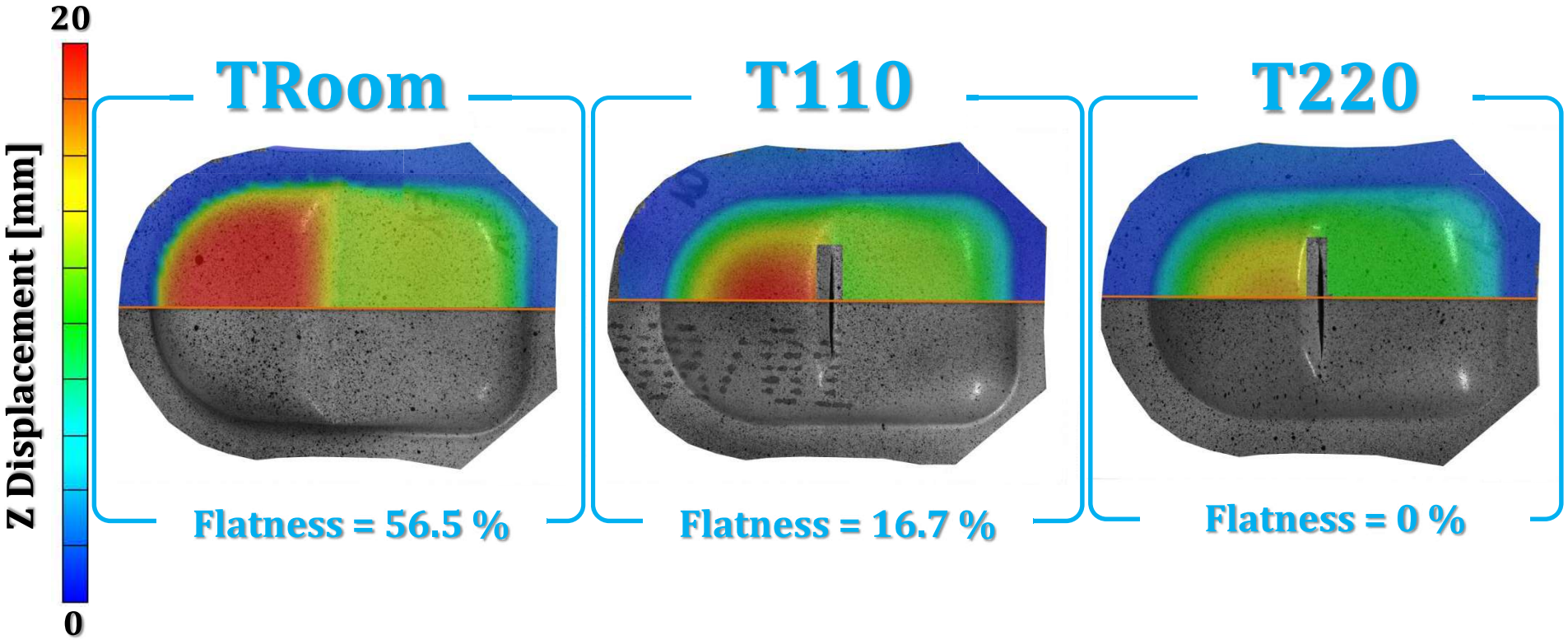
20
Z Displacement [mm]
0
TRoom
T110
T220
Flatness = 56.5 %
Flatness = 16.7 %
Flatness = 0 %

Figure 14a

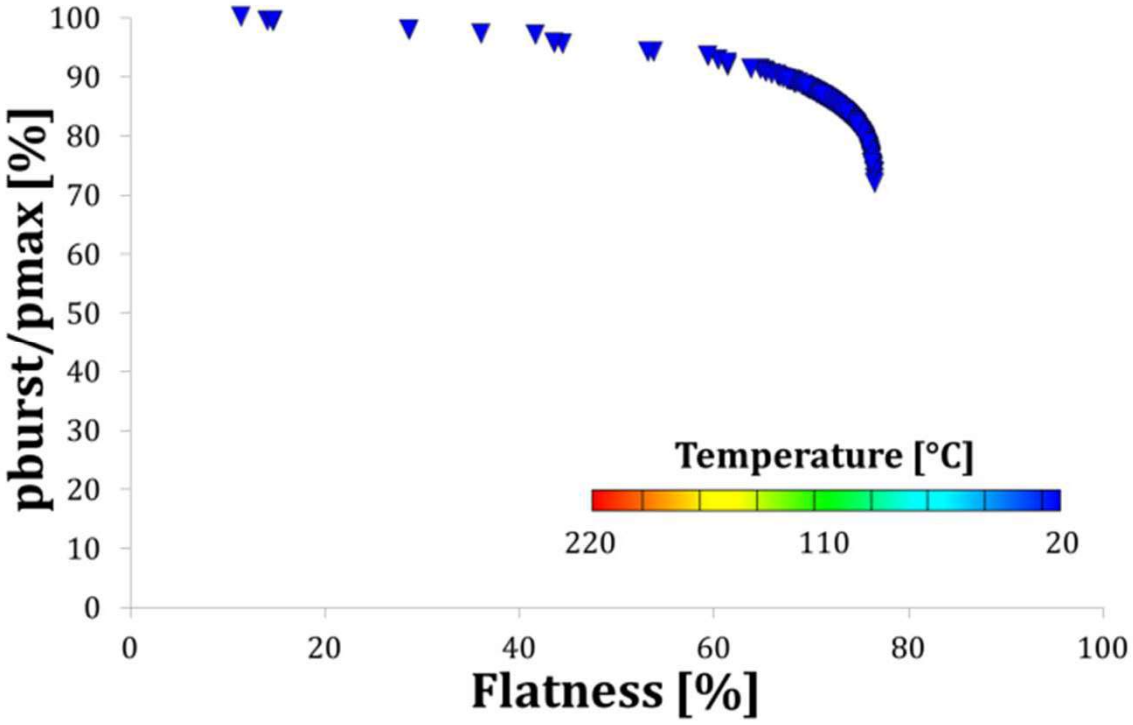
pburst/pmax [%]
100
90
80
70
60
50
40
30
20
10
0
0
20
40
60
80
100
Flatness [%]
Temperature [°C]
220
110
20

Figure 14b

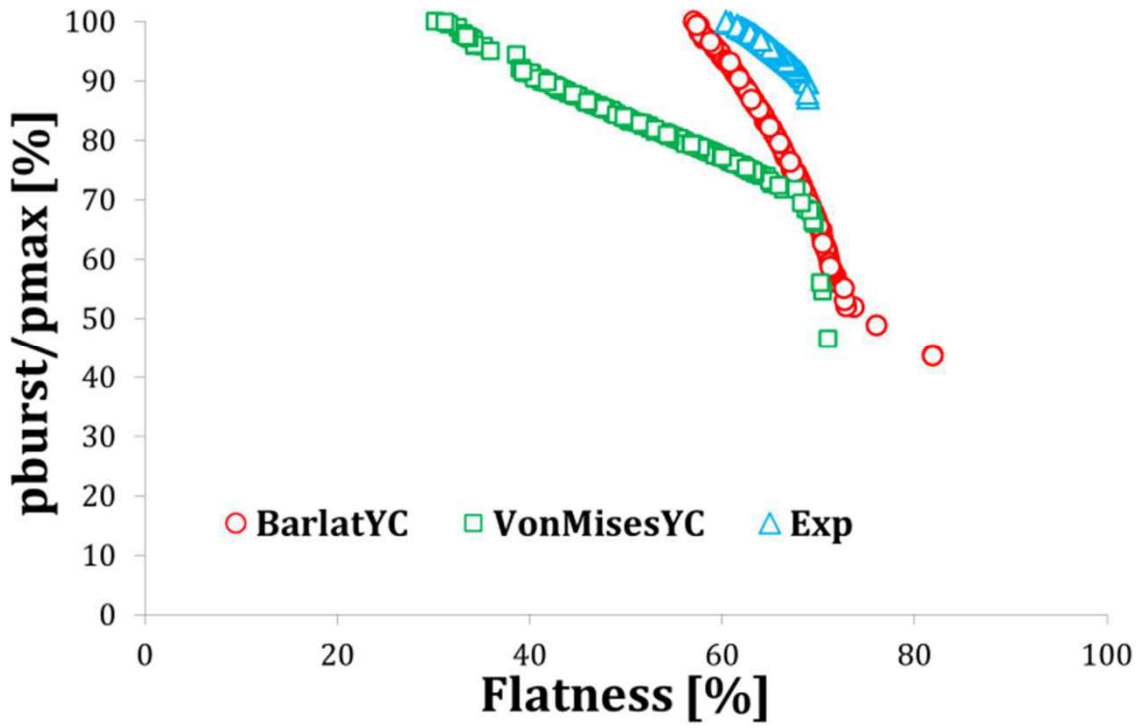
pburst/pmax [%]
100
90
80
70
60
50
40
30
20
10
0
0
20
40
60
80
100
Flatness [%]
BarlatYC
VonMisesYC
Exp